

NUREG/IA-0053



International Agreement Report

An Assessment of TRAC-PF1/MOD1 Using Strathclyde 1/10 Scale Model Refill Tests 2nd Report

Prepared by
W. M. Dempster, A. M. Bradford, T. M. S. Callander, H. C. Simpson

University of Strathclyde/Central Electricity Research Laboratories
Kelvin Avenue
Leatherhead, Surrey
United Kingdom

Office of Nuclear Regulatory Research
U.S. Nuclear Regulatory Commission
Washington, DC 20555

March 1992

Prepared as part of
The Agreement on Research Participation and Technical Exchange
under the International Thermal-Hydraulic Code Assessment
and Application Program (ICAP)

Published by
U.S. Nuclear Regulatory Commission

9204060332 920331
PDR NUREG
IA-0053 R PDR

NOTICE

This report was prepared under an international cooperative agreement for the exchange of technical information.* Neither the United States Government nor any agency thereof, or any of their employees, makes any warranty, expressed or implied, or assumes any legal liability or responsibility for any third party's use, or the results of such use, of any information, apparatus product or process disclosed in this report, or represents that its use by such third party would not infringe privately owned rights.

Available from

Superintendent of Documents
U.S. Government Printing Office
P.O. Box 37082
Washington, D.C. 20013-7082

and

National Technical Information Service
Springfield, VA 22161

NUREG/IA-0053



International Agreement Report

An Assessment of TRAC-PF1/MOD1 Using Strathclyde 1/10 Scale Model Refill Tests 2nd Report

Prepared by
W. M. Dempster, A. M. Bradford, T. M. S. Callander, H. C. Simpson

University of Strathclyde/Central Electricity Research Laboratories
Kelvin Avenue
Leatherhead, Surrey
United Kingdom

Office of Nuclear Regulatory Research
U.S. Nuclear Regulatory Commission
Washington, DC 20555

March 1992

Prepared as part of
The Agreement on Research Participation and Technical Exchange
under the International Thermal-Hydraulic Code Assessment
and Application Program (ICAP)

Published by
U.S. Nuclear Regulatory Commission

NOTICE

This report is based on work performed under the sponsorship of the United Kingdom Atomic Energy Authority. The information in this report has been provided to the USNRC under the terms of the International Code Assessment and Application Program (ICAP) between the United States and the United Kingdom (Administrative Agreement - WH 36047 between the United States Nuclear Regulatory Commission and the United Kingdom Atomic Energy Authority Relating to Collaboration in the Field of Modelling of Loss of Coolant Accidents, February 1985). The United Kingdom has consented to the publication of this report as a USNRC document in order to allow the widest possible circulation among the reactor safety community. Neither the United States Government nor the United Kingdom or any agency thereof, or any of their employees, makes any warranty, expressed or implied, or assumes any legal liability of responsibility for any third party's use, or the results of such use, or any information, apparatus, product or process disclosed in this report, or represents that its use by such third party would not infringe privately owned rights.

SUMMARY

TRAC PF1/MOD1 predictions of LOCA refill experiments carried out on a 1/10 scale model are presented and compared against experimental measurements and video observations. Sensitivity studies have been carried out to determine the effect of hydraulic diameter and nodalisation. It has been shown that a 4 segment mesh is insufficient to represent the geometry and phenomena in the downcomer during the refill process. It is suggested that improper modelling of the vessel/pipe connections causes the incorrect prediction of the distribution of injected liquid. Therefore, the liquid fraction at and below the injection positions is over-predicted with the consequences of the incorrect calculation of interfacial momentum and energy transfer terms.

A simplified analysis of total penetration conditions reveals that the liquid heat transfer coefficient during condensation is substantially greater than suggested by the reduction of the experimental measurements.

CONTENTS

	Summary	iii
	Contents	v
	Nomenclature	vii
1.	Introduction	1
2.	Sensitivity Study: Hydraulic Diameter	1
3.	Assessment of TRAC Interfacial Heat Transfer Correlations	3
4.	Nodalisation Study	6
5.	Discussion of Results	12
6.	Conclusions	14
7.	Recommendations for Further Study	15
8.	References	16
	Acknowledgements	17
	Appendices	18

NOMENCLATURE

A	Surface Area (m^2)
B	Interfacial area per unit length (m)
α	Void Fraction
C_p	Specific heat capacity (J/kgK)
D	Diameter (m)
E	Entrainment Fraction
g	Gravitational acceleration (m/s^2)
h_{fg}	Enthalpy of evaporation (J/kgK)
h	Heat transfer coefficient (Watts/ m^2K)
Ja	Jakob number.
k	Equilibrium Factor
M	Mass Flow (kg/s)
p	pressure (N/m^2)
ΔT_{sub}	Inlet subcooling (saturation temp - inlet water temp) (K)
v	Velocity (m/s)
W	Circumference (m)
y	Fraction of inlet water penetrating to lower plenum.
μ	Dynamic viscosity (Ns/m^2)
Γ	Surface tension (N/m)
ρ	density (kg/m^3)
$\Delta\rho$	$\rho_l - \rho_g$ (kg/m^3)
ΔX	cell length (m)

Subscripts

d	droplet
dc	downcomer
h	hydraulic
i	interfacial
in	inlet
l	liquid
LP	Lower plenum
r	relative
s	steam
sat	saturated
v	vapour

1. INTRODUCTION

This report describes the second and final phase of an investigation to assess the capabilities of the thermal hydraulic code TRAC PF1/MOD1 to simulate the refill phase of a double ended cold leg break LOCA. An initial investigation (Ref.1) established the codes poor predictive performance when applied to steady state refill experiments carried out at Strathclyde University on a 1/10 scale model of a PWR downcomer. However, an improvement in the TRAC predictions was obtained when the convective terms in the momentum equations were reformulated in a more conservative form. The calculations reported in this document continue from the previous work and attempt to address some of the questions that arose over TRAC'S sensitivity to nodalisation and the appropriate hydraulic diameter for the downcomer flow paths. In addition a limited assessment of the interfacial heat transfer modelling has been carried out against the Strathclyde experimental data.

The experimental facility was previously reported (Ref.1). However, for completeness a line diagram of the facility is shown in Fig. 1.1 and details of the 1/10 scale vessel are shown in Fig. 1.2. The TRAC nodalisation of the test facility is shown in Fig. 1.3 and is used in all TRAC calculations.

2. SENSITIVITY STUDY: Downcomer Hydraulic Diameter

2.1 Background

During the previous study (Ref.1) various questions arose concerning the difficulty of modelling the particular design of downcomer simulated in the 1/10 scale model. A thermal shield is incorporated into the downcomer annulus and this divides the downcomer into two separate flow paths; an inner gap of 6 mm and an outer gap of 13 mm (Fig.1.2). The flow conditions could only be fully resolved by using at least 2 rings in the numerical solution grid to represent the downcomer. However, this would introduce a substantial increase in cpu time and still not remove the uncertainty in the prediction since TRAC would then have difficulty in predicting the correct division of flows between the channels. To overcome some of these difficulties the downcomer was modelled with one ring in the numerical grid and the flow areas of the two channels were combined into a single flow path. A difficulty then arises when specifying an appropriate hydraulic diameter for the downcomer which through the TRAC constitutive relations affects the calculation of wall shear stress, wall to fluid heat transfer and interfacial shear stress and heat transfer.

Two sets of calculations were performed to quantify the effect of this parameter on the solution. The first, which was discussed in detail in the previous report (Ref.1) was performed with a hydraulic diameter of twice the combined gap size (0.038m). This effectively ignored the presence of the thermal shield. To determine the effect of this modelling assumption a series of calculations were repeated with the thermal shield surface area taken into account. This produced a hydraulic diameter of half the original (0.019m).

The refill experiments used for this sensitivity test are identified in Table 2.1. The original tests with a hydraulic diameter of 0.038 m are identified as B, C and D, the repeated tests with a hydraulic diameter of 0.019 m as B2, C2 and D2, respectively. Figs. 2.1 - 2.6 compare the differences in the TRAC results for each of the tests and are discussed separately below.

2.2 *TRAC Calculations*

Steam/Water Partial Penetration Tests B/B2

It can be seen from Fig. 2.1 that reducing the hydraulic diameter has produced a much improved prediction of the bypass flow rate. However the the flow conditions in the downcomer are still incorrectly predicted as can be deduced from the reduction in the calculated overall steam condensation rate when compared with the experimental measurement. (Fig.2.2). In addition, the wall heat transfer has decreased, as shown in Fig. 2.3 which is likely to be associated with the reduction in liquid in the downcomer.

Air/Water Partial Penetration Tests C/C2

Fig. 2.4 shows that changing the hydraulic diameter had very little effect on the results of this test, the prediction remaining a very poor simulation of the actual test.

Steam/Water Total Bypass Tests D/D2

Fig. 2.5 shows that from 12 seconds onwards the overall result changed from a partial bypass situation to a total penetration condition. Also the path chosen by TRAC for liquid to flow to the lower plenum switched from sector 7 to sector 8 for no apparent reason. (Fig 2.6).

2.3 *Discussion*

It is apparent from the above tests that using a more appropriate value of the hydraulic diameter did not produce any improvements in the predictions of the experimental tests.

However, it did indicate how TRAC can be sensitive to parameters such as the hydraulic diameter. Also, the results of test B/B2 show that the prediction depends on the interaction of many effects which all have to be adequately modelled to correctly predict the refill conditions. In TRAC the hydraulic diameter influences, to varying degrees interfacial heat transfer, interfacial friction, wall to fluid heat transfer and wall friction (Ref. 2). Identifying how each of these model dependencies affect the results is an almost impossible task at the level of analysis that is currently being carried out. This would require a much more detailed analysis and a more flexible code to assess TRAC's difficulties in simulating the phenomena observed during refill conditions. An example of such enhancements would be the capability to output the individual terms of the momentum equations, condensation rates, heat transfer coefficients, etc. as part of the graphics dump. This ability to control the output of calculated parameters would allow a more detailed analysis to be carried out.

3. ASSESSMENT OF TRAC INTERFACIAL HEAT TRANSFER CORRELATIONS

3.1 *Overview*

In any TRAC assessment using separate effects tests such as the Strathclyde refill tests, a difficulty arises in identifying deficiencies with individual physical models used in the code due to the interdependency of other effects. For Steam/Water tests with substantial liquid subcooling the TRAC predictions are the result of the effects produced by the interfacial heat transfer, interfacial friction, wall friction and wall to fluid heat transfer models. These tests involve too many effects for code deficiencies to be easily identified.

This section attempts to overcome this difficulty by restricting the comparison to total penetration conditions where the flow regimes are known with some confidence, and the experimental measurements can be reduced to give interfacial heat transfer coefficients. The appropriate TRAC interfacial heat transfer models for these conditions can be extracted from the TRAC code and assessed separately.

3.2 *Analysis*

The Strathclyde experiments covered a range from complete bypass to complete penetration of the inlet liquid flow. It was apparent from the video recordings that for most bypass conditions, particularly with any substantial liquid subcooling, highly chaotic flow regimes existed in the downcomer. However, for total penetration conditions the flow

regime was less disturbed and existed as a downward flowing liquid film attached to the downcomer wall with a counter current flowing vapour. Under these conditions it is possible to approximate the interfacial area within the following limits:

$$A_{ik} \leq A_i \leq 2 A_{ik}$$

i.e. the film will either exist on one wall or both walls, therefore doubling the interfacial area for the liquid film.

Therefore, since the flow regime interfacial area can be quantified for these conditions it is possible to compare the TRAC condensation models for the total penetration flow regime. The particular TRAC models being compared here are described in (Ref.2) and only relate to the film condensation models. This comparison does not include the models associated with droplet heat transfer nor the special models implemented to account for the jet flow regimes at the cold leg/vessel injection points (Ref.3). The TRAC models being assessed are described below and will be compared in the following form.

$$hA_{trac} = h_{i, film} A_{i, film}$$

where $h_{i, film} = 0.02 \rho_l C_{p_l} V_1$

$$A_{i, film} = \text{MAX} \left(\left[\pi D_h \Delta X \frac{1-\alpha}{1-2\text{DUK}} \right], \text{SLABAREA} \right) 2$$

$$\text{DUK} = 1 - \frac{10^{-3}}{D_h}$$

To carry out the assessment, the interfacial area has been identified as double the inside downcomer wall area (i.e. 2 x SLAB Area) and the entrainment set to zero. However it should be noted that if TRAC was being used to model downcomer conditions in which the slab area was not included (i.e. SLAB AREA = 0.0) in the input decl. then the interfacial film area would be wrongly evaluated and represented by a cylinder of diameter D_h and length ΔX instead of the considerably larger downcomer wall surface area.

Also V_1 has been calculated from

$$V_1 = \min \left(\frac{M_l}{A_{dc} \rho_l (1-\alpha)}, 3.0 \right)$$

The method used to reduce the experimental measurements of condensation rates to interfacial heat transfer coefficients has been discussed by Lieu et al (Ref.4) and extended more recently by Megahed (Ref.5, 6). The following expression relates the heat transfer coefficient and interfacial area product to the experimental conditions. An outline of the derivation for this expression can be found in Appendix 1.

$$h_i A_i = -\ln(1-k) M_i C_{p_i}$$

$$\text{where } k = \text{equilibrium factor} = 1 - \exp\left(-0.24\left(Ja_j^* \left(\frac{\rho_l}{\rho_v}\right)^{1/2} y^{-1/2}\right)^{-0.6}\right)$$

$$j_i^* = \frac{M_i}{A \rho_l} \sqrt{\frac{\rho_l}{g W (\rho_l - \rho_v)}}$$

$$Ja = \frac{C_{p_i} \Delta T}{h_{i,fl}}$$

The above expressions were used to calculate the heat transfer coefficient area product for the range of inlet liquid flow rates covered by the Strathclyde experimental tests i.e. 0 - 8 kg/s. It should be noted that the Strathclyde expression for the equilibrium factor was found to be dependent on the degree of inlet subcooling while the TRAC models are not. Therefore to indicate the range of possible values for the experimental $h_i A_i$, subcoolings of 20 K and 60 K have been used to produce the two curves shown in Fig.3.1 which are compared with the TRAC computed values of $h_i A_i$.

It is quite apparent from Fig.3.1 that the TRAC condensation heat transfer rates can be an order of magnitude higher than the experimentally derived values.

3.3 Condensation Models Characteristic

An exercise was carried out to examine the general characteristics of the condensation models incorporated in the TRAC code. The correlations used were those corresponding to the annular mist condensation models and are described in Appendix A2. Fig. 3.2 shows the variation of the individual film and mist components of equation A.2.1 and the total heat transfer coefficient area product ($h_i A_i$) with vapour velocity. It can clearly be seen that already high values associated with the liquid film coefficient increase rapidly for an increase in the vapour velocity. This increase is due to the increased entrainment over this velocity range and is similar to the increase in interfacial drag discussed in the previous

report (Ref.1). In addition Fig. 3.3 shows how the heat transfer rate will decrease as void fraction is increased mainly due to the decrease in interfacial surface area between the liquid and the vapour.

4. NODALISATION STUDY

4.1 *Background*

Previous TRAC assessments (Ref. 8, 9) had attempted to investigate the effect of nodalisation changes but no conclusion could be made to support any particular degree of nodalisation. Cappiello (Ref.8) had conducted a limited study by increasing the number of circumferential sectors from four to eight and reported that this had no effect on the results. However, Slovik (Ref.9) had carried out nodalisation sensitivity studies by concentrating on the effect of the flow area blockages associated with the hot leg penetrations and found TRAC to be very sensitive to how the blockages are modelled but with no clear trend emerging on how the blockages affect the overall results.

The current exercise investigates the effect of nodalisation on the TRAC calculations using a limited number of numerical grid changes. Only the total bypass test, (test D of the previous tests, Ref.1) was used to investigate grid changes so to minimise on cost but to maximise on grid variations. The choice of nodalisation was primarily based on an analysis of the TRAC calculations carried out in the previous Phase I study (Ref.1). In these calculations it was observed that variables such as the vapour velocity could increase from values of 15 m/s at the downcomer entrance to over 30 m/s at the cold leg break cell position [Sect 5, Level 11]. However, the vapour velocity in the cold leg break pipe was usually in the region of 60-70 m/s which suggested that much greater velocities were present in the downcomer than the calculated 30 m/s. Steep gradients also existed in the circumferential direction but with a much coarser circumferential grid than the axial direction. In addition, the liquid in the downcomer tended (in total bypass conditions) to be concentrated at the top of the downcomer where the existing grid was very coarse. It should also be noted that it is impossible to fully resolve the cold and hot leg vessel geometry in the downcomer of a 4 loop PWR with a 4 sector model, due to the difficulty of correctly positioning the cold leg positions relative to the broken cold and hot leg penetration.

As has been pointed out in the previous study (Ref.1) and in section 2 of this report, the interfacial heat transfer and shear stress are very sensitive to the magnitude of the vapour velocities. In fact for large relative velocities the heat transfer is proportional to the square of the vapour velocity while the shear stress is proportional to the fourth power of the vapour velocity. In addition these two important parameters are also dependent on the void fraction in the determination of interfacial areas and flow regimes. The overall effect is likely to produce a calculation that is very sensitive to the vapour velocities and flow regimes.

This exercise has two basic objectives:

- (1) to determine the effect of refining the numerical grid circumferentially and axially. This would investigate the effect on numerical approximations, i.e. whether the solution had converged and to investigate the circumferential positioning of the cold leg injection points relative to the break;
- (2) to investigate the effect of including hot leg penetrations which are modelled as flow area blockages in TRAC.

4.2 TRAC CODE

The TRAC code used in this exercise was a version of the Winfrith TRAC, B Ø3, modified by Turner (Ref.10) to include a more conservative formulation of the finite difference equations. However, ambiguity arose over the extent of the modifications to the convection terms in the TRAC momentum equations for the liquid and vapour phases. Therefore, the equations are outlined below for clarity.

The original formulation of the TRAC momentum equations for the vapour Z-direction equation are:

$$\frac{\partial u_z}{\partial t} + u_r \frac{\partial u_z}{\partial r} + \frac{u_\theta}{r} \frac{\partial u_z}{\partial \theta} + u_z \frac{\partial u_z}{\partial z} + \frac{1}{\rho} \frac{\partial p}{\partial z} = [\text{TERMS}]$$

Turner modified the equations by reformulating the main convection term $\left(eg. u_z \frac{\partial u_z}{\partial z} \right)$ in each direction of the vapour and liquid momentum equations. Thus the above equation became:

$$\frac{\partial u_z}{\partial t} + u \frac{\partial u_z}{\partial r} + \frac{u_\theta}{r} \frac{\partial u_z}{\partial \theta} + \frac{1}{\alpha \rho} \frac{\partial}{\partial z} (\alpha \rho u_z^2) + \frac{1}{\rho} \frac{\partial p}{\partial z} = [\text{TERMS}]$$

An attempt was made by Turner to reformulate other convection terms (eg $\frac{u}{r} \frac{\partial u_z}{\partial \theta}$, $\frac{u_\theta}{r} \frac{\partial u_z}{\partial \theta}$)

However, coding difficulties excluded this work from being completed in time to be used in this study.

4.3 *Vessel Nodalisation*

The numerical grids chosen for the vessel nodalisation reflected our understanding that the steepest gradients of the dependent variables, velocity, temperature, void fraction etc. were concentrated in the upper downcomer region for a total bypass test. Table 4.1 shows the range of tests carried out. In Tests S1, S2 and S3 the circumferential sectors were increased from 4 to 8 to 16 respectively for a 13 level grid, while in Tests S2, S5, and S6 the effect of an increase in axial levels was investigated for an 8 sector grid. The effect of flow area blockages was investigated in a 15 level grid for Tests S7, S8 and S9 while the consequence of moving cold leg positions was shown in Test S10 for a 4 sector nodalisation.

Figs. 4.1, 4.2 and 4.3 show the axial levels for Tests S1, S2 and S3. Fig. 4.2 and Table 4.1 also show the position of the blockages used in Tests S7, S8 and S9. Figs. 4.4a, 4.4b, 4.4c and 4.5 show the circumferential positions of the cold legs in each test.

4.4 *Steady State Vapour Only Condition*

One of the most difficult problems in analysing the source of differences between tests is the number of and variation in the dependent variables of the problem. To minimise these difficulties it was thought judicious to study the effect of the vapour velocity during the initial single phase period (0 - 5 secs.) of the calculation prior to water injection. This would highlight the effect of the nodalisation changes and give some indication of the appropriateness of the chosen numerical grid. However, even though the single phase vapour velocity distribution will be similar to that during the transient, the existence of liquid and localised condensation will further introduce transient redistribution of the vapour velocity and necessitate the need for a finer numerical grid than that appropriate for the steady state single phase condition.

An examination of the effects of increasing the number of circumferential sectors from 4 to 16 (Tests S1, S2 and S3) show that the solution has clearly not converged. Figs. 4.6, 4.7 and 4.8 show the vapour velocity components for the axial and circumferential directions of each top and right hand face respectively, for each cell. The velocity components, in particular geometrical planes, have been taken from the values shown in Figs. 4.6, 4.7 and 4.8 to produce the curves in Figs. 4.9, 4.10 and 4.11.

Fig. 4.9 shows the axial velocity components directly below the break cell (ie levels 4 - 10, Fig. 4.1) for each of the grid changes. It can be seen that an increase in the number of circumferential sectors produces greater velocities in regions close to the break cell. Fig. 4.10 shows the axial velocity components up the downcomer in the circumferential sector furthest from the break. The decrease in the axial component of velocity is indicated quite clearly in the upper downcomer regions as the grid is refined in the circumferential direction.

Fig. 4.11 shows the effect of the circumferential grid changes on the circumferential velocity component and plots the theta velocity components around the downcomer from the break cell position, at the break cell level. It can be seen that higher velocity magnitudes are predicted close to the break and is similar to the effects on the axial velocity component. Better predictions of the circumferential velocity component associated with the line of symmetry in the flow field at 180 degrees are being produced. However, the calculation using the 13:16:2 grid shows a slightly skewed velocity distribution with the line of flow symmetry appearing at 126 degrees from the break instead of 180 degrees. The asymmetry in the flow is believed to be caused by the way the steam was introduced into the vessel. The steam mass flow entered into the core via a hot leg and since this pipe/vessel connection used only one core sector, an asymmetry in the flow could be produced as the grid was refined in the circumferential direction. The asymmetry in the core flow could then easily propagate into the downcomer.

Similar trends in the velocity distribution can be seen by increasing the axial levels from 13 to 15 for an 8 sector grid and concentrating the increase in the levels to the cold and hot leg region (see Fig. 4.2 for nodalisation). Fig. 4.12 shows the vapour velocity components in the axial and circumferential directions with the spatial effects plotted in Figs. 4.9, 4.10 and 4.11.

Comparing Tests S5 and S9 which show the effects of introducing flow area blockage, as indicated in Fig. 4.2 it can be seen that the main differences were localised to the break area. Fig. 4.13 shows the redistribution of the vapour flow as it leaves the blockage regions.

Therefore, it can be seen from the above assessment of the single phase vapour flow distribution that as the numerical grid is refined, particularly in the circumferential direction and axially local to the break, the vapour velocities reduce in the regions furthest from the break and increase local to the break.

However, refining the numerical grid in the circumferential direction improves the ability to model the correct position of the cold leg, vessel connections. The consequences of this are that the ECC injection flow enters into regions of lower vapour velocities, in particular circumferential velocity components, when compared to the four sector coarse grid. The ability to bypass the liquid would then be expected to diminish.

4.5 *Transient Steam-Water Flows*

The transient cases tend to be more difficult to analyse since the change in the numerical solution grid affects each of the dependent variables. The combined effect may result in a widely different solution depending on the sensitivity of the calculation to the dependent variables.

Figs. 4.14 to 4.18 show the break mass flow rates for the cases chosen to investigate an increase in the number of cells in the solution grid but with the exclusion of any hot leg blockage modelling; Tests S1, S2, S4, S5 and S6. Changing from a 13:4:2 to 15:4:2 grid did not change the overall result, i.e. total bypass was predicted in both cases as can be seen from Figs. 4.14 and 4.18. Though the liquid is being held up in the upper downcomer for both cases, (Fig. 4.20, 4.21) it is more uniformly distributed as would be expected with the greater number of axial levels in this area.

Changing from a four sector to an eight sector grid resulted in a reduction in the break mass flow, as can be seen in Fig. 4.15 which shows the calculation for Test S2, a 13:8:2 grid. Changing the axial levels for an 8 sector grid produced similar break flowrates, as is shown in Figs. 4.15, 4.16 and 4.17.

However, an interesting result is indicated in Fig. 4.22 which shows the lower plenum filling characteristics for calculations using an 8 sector grid, Tests S2, S5 and S6. As the axial levels were increased from 13 to 18, the time for liquid to penetrate the downcomer was reduced by just over 4 seconds.

It should be noted that by changing from the 4 sector grid to the 8 sector grid the cold leg connections are repositioned further from the break. Different flow conditions in the downcomer can therefore be produced. An example of this can be seen in Fig. 4.23 which shows the steam condensation rates in the downcomer averaged between the injection points and the bottom of the downcomer. (i.e. levels at 1.067 m and 0.173 m) for 15:4:2 and 15:8:2 grids. It can be seen that the changes have increased the condensation rates for the 15:8:2 grid and is therefore a contributing factor to the over prediction of the lower plenum flows for this total bypass test.

The affect of introducing flow area blockages to model the hot leg penetrations was investigated by performing Test S7, for a 15:4:2 grid and Tests S8 and S9 for 15:8:2 grids, (Table 4.1). Fig. 4.19 shows the results of the 15:4:2 grid calculation. When compared to Fig. 4.18, which shows the results of a similar calculation but without hot leg blockages, it can be seen that total liquid bypass was correctly predicted in both cases. Figs. 4.18 and 4.19 also indicate that steady flow conditions were produced after 16 secs for Test S4 while no such trend was repeated when the hot leg blockages were modelled, (Test S7).

However, similar calculations using a 15:8:2 grid showed that significant differences in the results could occur. By comparing Figs. 4.15, 4.24 and 4.25, which show the break mass flow rates for Tests S2, S8 and S9 respectively, it can be seen that liquid bypass is sustained for much longer periods as the degree of flow area blockage is increased for the 15:8:2 grid.

The above blockage tests (S8 and S9) provided interesting results when the downcomer flow pattern was analysed in some detail. By using the graphical animation software developed at Strathclyde the results were by far the most realistic of all the calculations yet performed when compared with the experimental observations of the downcomer flows using the flow visualisation video recordings obtained during the original tests.

It can be seen how the TRAC predictions of oscillatory flow can be related to the multi-dimensional flow distribution in the downcomer. As an example, the break flow cycle shown in Fig. 4.25 over the time period 9 - 12 seconds can be related to a build up of liquid in downcomer region furthest from the break which collapses and flows towards the lower plenum. The liquid is then swept circumferentially and upwards, towards and out of the break. This appears as a two second cycle in which the break mass flow rate reduces as the majority of the liquid flows towards the lower plenum and increases as the liquid is swept back up the downcomer and out of the break. This sequence of events is shown in Figs. 4.26 to 4.29.

The question arose as to the reasons why the 4 sector grid predicted total liquid bypass and whether the position of the cold legs were important. Therefore a calculation was performed (Test S.10) with the cold legs repositioned as in Fig.4.5 (which is more geometrically correct for a 4 sector nodalisation than shown in Fig.4.4a) Fig. 4.30 shows the break mass flow for Tests S1 and S10 and it can be seen that TRAC overpredicts the amount of liquid penetrating the downcomer, again indicating the importance of correctly modelling the position of the cold leg connection.

4.6 TRAC Computational Efficiency

The CPU time of each calculation can be used as an overall gauge of the computational efficiency with which TRAC predicts the particular phenomenon under study. Fig. 4.31 shows the CPU time versus real time for four typical calculations during the sensitivity study. It can be seen that increasing the numerical grid from a 13:4:2 grid to a 15:8:2 grid has produced an almost nine fold increase in the CPU time to a magnitude of 9000 seconds for Test S9. This is obviously an undesirable level of performance implying high costs which impose limits on the number of studies that can be carried out. Fig. 4.32 shows the time steps used during the calculations and it can be seen that for most of the calculations the time step varied between 1.5 to 3×10^{-3} secs. This was identified as the CFL (Courant Freidricks Lewy) stability limit for the calculations.

5. DISCUSSION OF RESULTS

From the previous three sections it is apparent that a number of physical models have to be simultaneously correct to adequately model the refill problem. Here the flow regime in the downcomer is determined by the main forces acting on the phases and the geometry of the downcomer. Since the momentum and energy transfer rates are closely related to the vapour velocities it is necessary to adequately resolve the velocity distribution in the downcomer. The importance of modelling the transient flow regime cannot be overstated since it determines not only the interfacial area but also the residence time of the liquid and therefore the liquid/steam contact time. This is then likely to have a bearing on the rate of liquid penetrating the downcomer. To simulate these conditions it is apparent from this study that the geometry of the downcomer has to be adequately represented. That is, the break has to be properly positioned relative to the other cold legs and the hot leg blockages modelled in some detail.

However, an examination of the flow distributions in the downcomer reveals that when the liquid flows towards the lower plenum it flows as a single liquid water column, in a one-dimensional manner down through downcomer levels. Fig. 4.27 is a good example of this. Even as the number of sectors increase the liquid continues to flow to the lower plenum in a single column (a 16 sector calculation of liquid entering via one cold leg was repeated with no steam flow to emphasise this characteristic and the single column flow trend was repeated). These results show that TRAC does not predict the 2-dimensional redistribution of the liquid as it flows downwards and therefore over predicts the liquid fraction in the injection region.

An examination of the TRAC momentum equation reveals that the circumferential forces acting on the liquid, to produce circumferential redistribution, are the shear forces produced by the circumferential vapour flows. However, the circumferential vapour flows are lower in the downcomer region furthest from the break and are likely to be insufficient to redistribute the liquid flow.

An examination of the Strathclyde air-water video indicates that for small air flows the water entering into the downcomer flows both circumferentially and downwards to meet the liquid flow distribution from the opposite cold leg. The redistribution of the liquid is associated with the deflection of the radially flowing liquid by the inside wall of the downcomer causing it to flow downwards under gravity and circumferentially due to the radial component of momentum of the cold leg flow. An example of this can be seen in Fig. 4.33 and 4.34 which show photographs of the incoming liquid redistributing around the 1/10 scale model downcomer.

However, the current formulation of the TRAC momentum equations is not capable of modelling this type of flow redistribution since no momentum convection terms are associated with a radial vessel/pipe connection (Ref.11). A limited study has been carried out by Turner (Ref.10) to implement momentum terms to account for this effect but with limited success. Unfortunately the study was only carried out with a 4 sector grid and there is therefore insufficient information on which to base any conclusion as to the appropriateness of Turner's proposed scheme.

It is suggested that this is possibly one reason why TRAC at times approaches the correct overall result though the flow regime is incorrect. Very high drag coefficients are produced for the bubbly flow regime ($\alpha < 0.3$), as shown in Fig. 4.35 (Ref.2) which could effectively redirect the flow upwards.

6. CONCLUSIONS

1. The use of the Strathclyde Refill experiments to assess TRAC's ability to simulate the refill conditions has limitations due to geometrical complications associated with the 1/10 scale model downcomer thermal shield.
2. A parametric study using two different downcomer hydraulic diameters to account for the thermal shield did not produce better results overall but did show that the TRAC predictions provide for complex interaction between wall heat transfer and interfacial shear and heat transfer.
3. A simplified analysis of the Strathclyde total penetration tests has shown that the TRAC liquid side heat transfer coefficient for the condensation process is an order of magnitude too great when compared with the experimentally derived values.
4. A nodalisation study has shown the effects of increasing the numerical solution grid. A 4 sector nodalisation does not provide a converged solution for the dependent variables.
5. For bypass conditions it is important to model the geometry of the break positions relative to the intact cold legs; hot leg penetrations make a significant contribution to the bypass process.
6. TRAC's inability to predict the circumferential redistribution of liquid injected into the downcomer due to the lack of appropriate terms in the momentum equations is a major deficiency in TRAC modelling.
7. TRAC's excessive computer run times is an important limitation in the progress to a possible solution of the downcomer flows during the refill phase.

7. RECOMMENDATIONS FOR FURTHER STUDY

1. Continue Turners work on the reformulation of the momentum equations to include the cross derivative terms for vessel/pipe connections.
2. Pursue improvements in TRAC's computational performance.
3. Improve interfacial modelling of shear stress and heat transfer.

8. REFERENCES

1. DEMPSTER, W.M., et al. An assessment of TRAC-PF1/MOD1 using Strathclyde 1/10 scale model refill results, Strathclyde University Report, Nov. 1988.
2. LILES, D.R., et al. TRAC-PF1/MOD1 Models and correlations, 1988 PWR/LCVSG/A(88).
3. LILES, D.R., et al. TRAC-PF1/MOD1: An advanced best-estimate computer program for pressurised water reactor thermal analysis NUREG/CR-3858, July 1986.
4. LIU, J.S.K., et al. Flooding of counter-current steam water flow in an annulus, ASME meeting, San Francisco, California, Dec. 10-15, 1978.
5. MEGAHED, M.M. Flooding and non-equilibrium in counter-current flows with reference to pressurised water reactors, PhD thesis, University of Strathclyde, Glasgow, U.K., Dec. 1981.
6. MEGAHED, M.M. Interfacial heat transfer in counter-current flows of steam and water, DOE-ID-10161, April 1987.
7. ROONEY, D.H., SIMPSON, H.C., MEGAHED, M.M. Non equilibrium effects in direct contact condensation during refill in a pressurised water reactor. Heat and fluid flow in nuclear and process plant safety. IMech. Conf., 1983.
8. CAPPIELLO, M. Assessment of the annular mist interfacial shear in TRAC-PF1/MOD1 against downcomer bypass and tie plate flooding data, 1985, ASME 84-WA/NT-84.
9. SLOVIK, G.C., SAHA, P. Independent assessment of TRAC-PF1/MOD1 code with BCL ECC bypass test, 1985, NUREG/CR-4252.
10. TURNER, D. A study of some discretisation effects in TRAC-PF1/MOD1 on the predictions of low subcooling counter-current flow, 1988, PWR/HTWG/P(88)592.
11. CODDINGTON, P., RICHARDS, C. Pressure losses at TRAC-PF1/MOD1 Component Boundaries. PWR/TUG/P(86)25.

ACKNOWLEDGEMENTS

The work described in this report was sponsored by the Central Electricity Generating Board. However the comments and conclusions contained within this report are those of the authors and may not represent the opinion of the sponsors. The authors would also like to express their thanks to D.M. Turner whose helpful discussions contributed to the progress of this work.

APPENDIX A.1

Figure A-1 shows a simplified model of a liquid film flowing down a wall adjacent to a counter-current flow of vapour. It is assumed that a one dimensional model is appropriate for these conditions and the effect of wall heat transfer to the liquid film is neglected. By applying the conservation laws for mass and energy across the differential section in conjunction with an energy balance across the liquid-vapour interface can lead to the expression for the amount of steam condensed at a position X along the wall, i.e.

$$M_{v, \text{con}} = M_{l, \text{in}} \frac{C_{pl}(T_{\text{SAT}} - T_{l, \text{in}})}{h_{fg}} \left(1 - e^{-\frac{Bx}{C_{pl} M_{l, \text{in}}}} \right) \quad \text{A.1.1}$$

This analysis has been carried out by Lieu (4) and extended to include wall heat transfer by Megahed (5).

Since
$$\frac{C_{pl}(T_{\text{SAT}} - T_{l, \text{in}})}{h_{fg}} = J_d$$

then
$$M_{v, \text{con}} = M_{l, \text{in}} \cdot J_d \cdot \left(1 - e^{-\frac{Bx}{C_{pl} M_{l, \text{in}}}} \right)$$

This can be reduced to

$$k = \frac{M_{v, \text{con}}}{M_{l, \text{in}} J_d} = \left(1 - e^{-\frac{Bx}{C_{pl} M_{l, \text{in}}}} \right) \quad \text{A.1.2}$$

where k is referred to as an equilibrium factor and represents the degree of thermal equilibrium as a fraction of the steam condensed to what would be required to reach thermal equilibrium.

A previous analysis of the Strathclyde experimental data (7) had already determined a correlation for the equilibrium factor as,

$$k = 1 - \exp \left(-0.24 \left[J_{aj} \cdot \left[\frac{\rho_l}{\rho_v} \right]^{1/2} y^{-1/2} \right]^{-0.6} \right) \quad \text{A.1.3}$$

Since Bx in equation A.1.2 represents the interfacial area A_i and if introduced into A.1.2 then equation A.1.2 and A.1.3 can be equated to provide a relationship for the heat transfer coefficient h or in our case the heat transfer coefficient interfacial area product, i.e.

$$hA_i = 0.24 \cdot C_{pl} \cdot M_{l, \text{in}} \cdot \left[J_{aj} \cdot \left(\frac{\rho_l}{\rho_v} \right)^{1/2} y^{-1/2} \right]^{-0.6} \quad \text{A.1.4}$$

It should be noted that equation A.1.4 is restricted by the assumptions made in the derivation of equation A.1.2. In the integration from the differential equations to equation A.1.1 the assumption of constant interfacial area was made. This therefore restricts the above equation to total penetration conditions where $y = 1$, i.e.

$$hA_i = 0.24 \cdot C_{p_i} \cdot M_{i,a} \left[\text{Ja}_i \right]^* \left(\frac{\rho_i}{\rho_v} \right)^{1/2} \left[\dots \right]^{0.8} \quad \text{A.1.5}$$

This expression can then be used to compare the TRAC values for the interfacial heat transfer coefficients against the experimentally determined values.

APPENDIX A.2

TRAC INTERFACIAL CONDENSATION MODELS FOR THE ANNULAR-MIST REGIME

The following equations describe the heat transfer correlations associated with the TRAC annular mist flow regime. The equations are restricted to the methods used to obtain the interfacial heat transfer coefficient and the interfacial area during condensation.

$$(h_i A_i)_{\text{annular mist}} = E(h_i A_i)_{\text{mist}} + (1 - E)(h_i A_i)_{\text{film}} \quad \text{A.2.1}$$

$$E = \text{entrainment factor} = \text{MAX}(7.75 \times 10^{-7} \times W_d^{1.25} \times \text{Re}_l^{0.25}, 1 - \exp\left(\frac{1}{2}\left(1 - \frac{V_v}{V_{\text{OLF}}}\right)\right))$$

$$W_d = \frac{\rho_l j_v^2 D_b}{\sigma} \left(\frac{\Delta\rho}{\rho_v}\right)^{1/3}$$

$$\text{Re}_l = \frac{\rho_l j_l D_b}{\mu_l}$$

$$V_{\text{OLF}} = 2.33 \frac{(\Delta\rho\sigma W_d)^{1/4}}{\sqrt{\rho_v}}$$

$$j_v = \frac{M_v}{\rho_v A} \left(\frac{\rho_v}{gW(\rho_l - \rho_v)}\right)^{1/2}$$

$$W_d = \frac{\rho V_l D_d}{\sigma}$$

$(h_i A_i)_{\text{film}}$ is the contribution of the film heat transfer where

$$h_i = 0.02 \rho_l C_{p_l} V_l$$

$$A_i = \text{MAX}\left(D_s \pi \cdot \Delta \times \frac{1 - \alpha}{1 - \text{DUK}}, \text{SLAB AREA}\right) \cdot 2$$

$$\text{DUK} = 1 - \frac{10^{-3}}{D_s} \quad 0 \leq \text{DUK} < \alpha$$

$(h_i A_i)_{\text{mist}}$ is the contribution of droplet heat transfer where

$$h_i = 0.02 \rho_i C_{pi} V_D$$

$$V_D = 1/2 \left(\frac{\mu_v}{\mu_v + \mu_l} \right) V_i$$

with the restriction that $V_D \leq \min \left(0.5, 1.4 \left(\frac{\rho_v}{\rho_l We_d} \right)^{1/2} V_i \right)$

$$A_{\text{mist}} = 6 (1 - \alpha) \frac{VOL}{D_d}$$

$$D_d = \frac{We_d \sigma}{\rho_v V_i^2}$$

TEST	EXP.ID	FLUID	$M_1(\text{kg/s})$	$M_2/M_1(\text{kg/s})$	$M_{1,p}(\text{kg/s})$	$\Delta T(K)$	$D_H(\text{m})$	TYPE	TRAC VERSION
B	01048023	Steam/Water	2.516	0.214	1.372	12.6	0.038	Partial Pen.	Winfrith B05
B2	"	"	"	"	"	"	0.019	"	"
C	15068168	Air/Water	7.65	0.266	1.984	0.0	0.038	Partial Pen.	Winfrith B05
C2	"	"	"	"	"	"	0.019	"	"
D	26038046	Steam/Water	4.888	0.403	0.0	37.6	0.038	Partial Pen.	Winfrith B05
D2	"	"	"	"	"	"	0.019	"	"

TABLE 2.1 TEST IDENTIFICATION FOR VARIATION IN HYDRAULIC DIAMETER

STRATHCLYDE TEST	FLUID	M_i (kg/s)	M_e (kg/s)	M_{LP} (kg/s)	ΔT (K)	TRAC VERSION	TEST TYPE
26038046	Steam/Water	4.888	0.403	0.0	37.6	Turner's: Bφ3	Total By-Pass

TEST	GRID Z:θ:R	HOT LEG MODELLING	Blockage Position
S 1	13 : 4 : 2	No Blockage	
S 2	13 : 8 : 2	No Blockage	
S 3	13 : 16 : 2	No Blockage	
S 4	15 : 4 : 2	No Blockage	
S 5	15 : 8 : 2	No Blockage	
S 6	18 : 8 : 2	No Blockage	
S 7	15 : 4 : 2	FA Blockage, θ	100% Flow Area Blockage at level 12 edge 5/6 and 7/8 Fig 4.4a
S 8	15 : 8 : 2	FA Blockage, θ	100% Flow Area Blockage at level 12 edge 10/11, 11/12, 13/14, 14/15 Fig 4.2
S 9	15 : 8 : 2	FA Blockage θ, Z	100% Flow Area Blockage as Test S8 and 51% axial blockage Fig 4.2
S10	13 : 4 : 2	Injection Points Changed	

TABLE 4.1 NODALISATION SENSITIVITY TEST SERIES FOR TEST 26038046

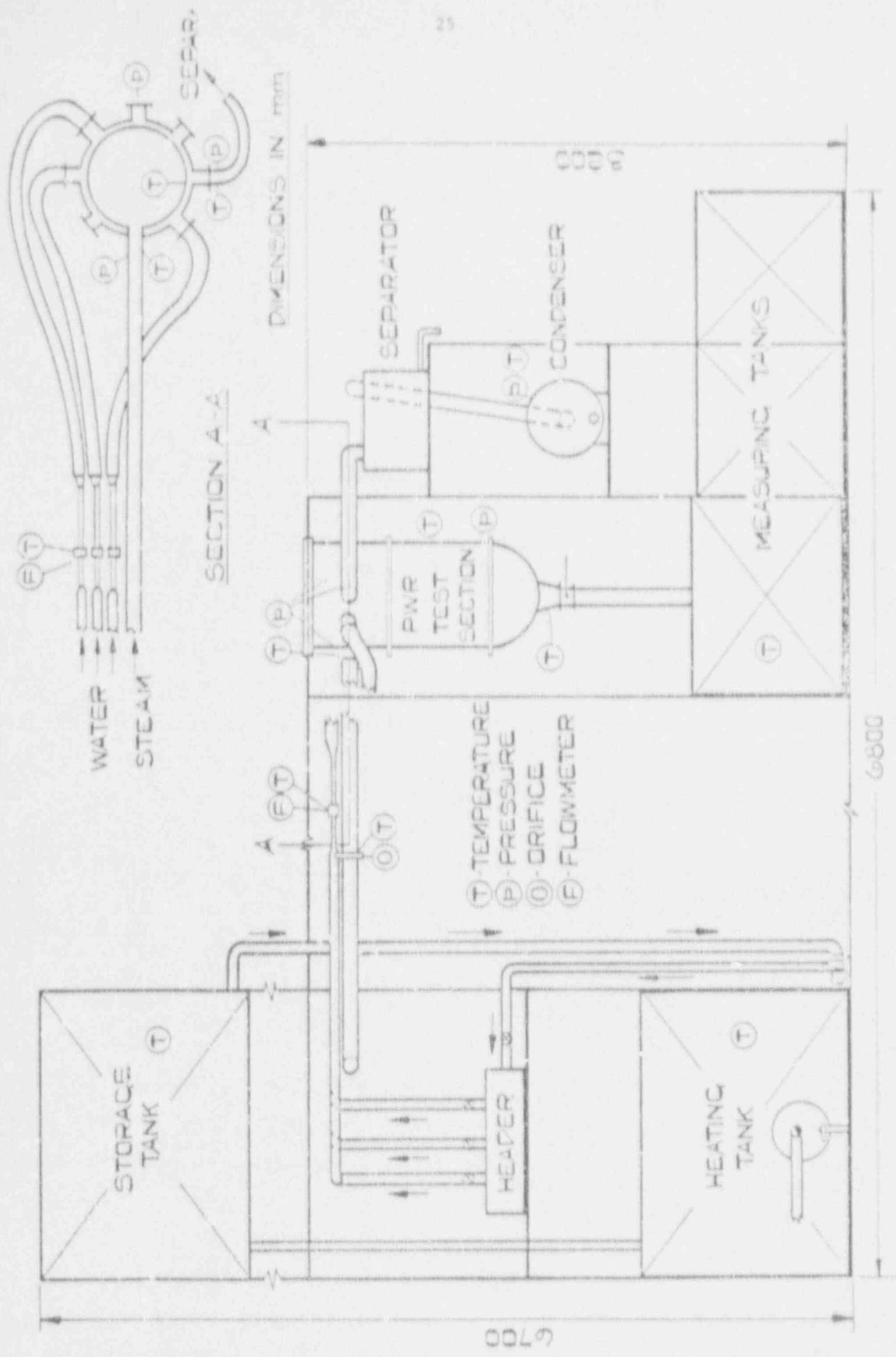
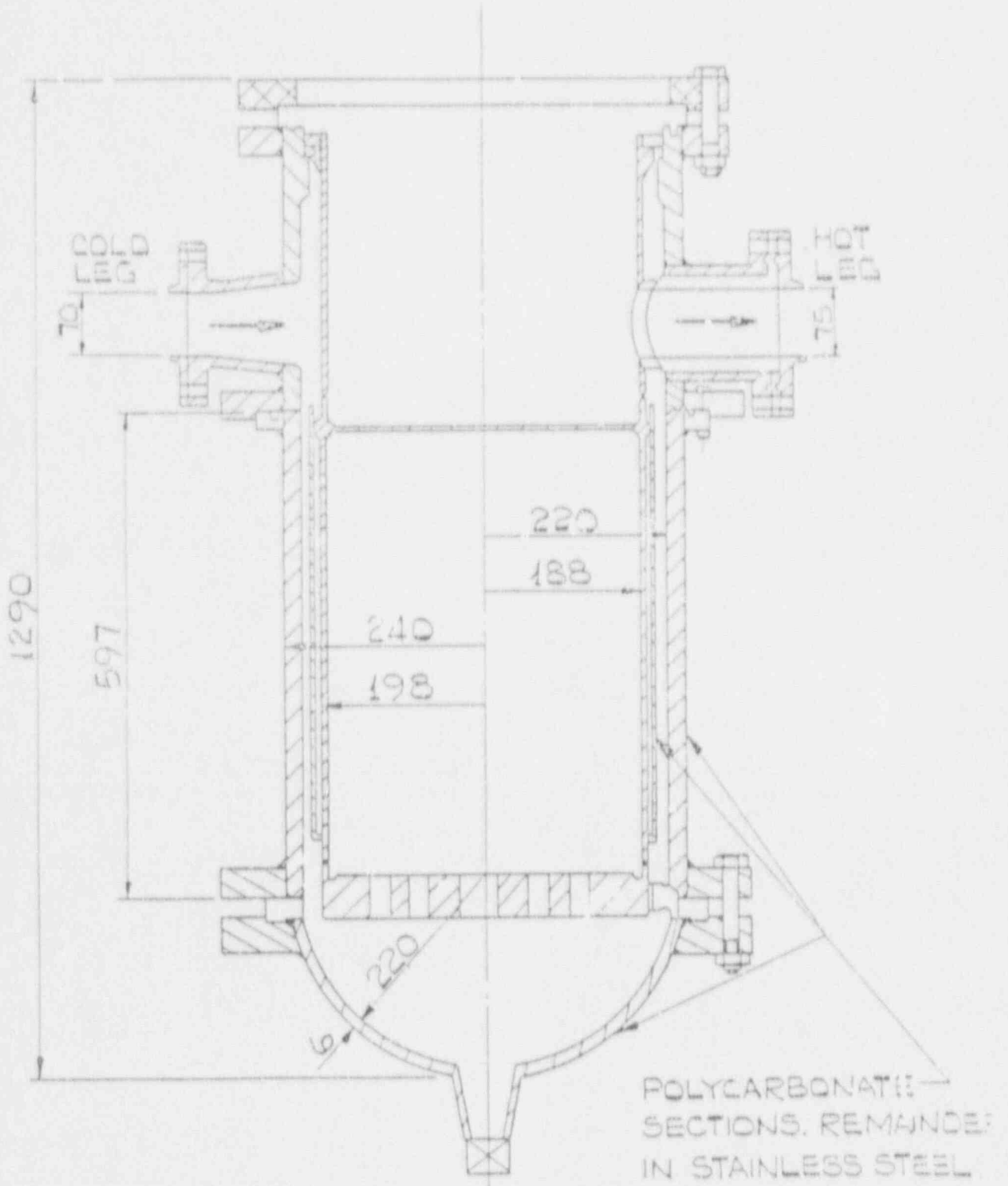


FIG.1.1 LAYOUT OF NEW PWR TEST RIG



DIMENSIONS IN mm.

FIG. 12 DETAILS OF TEST SECTION.

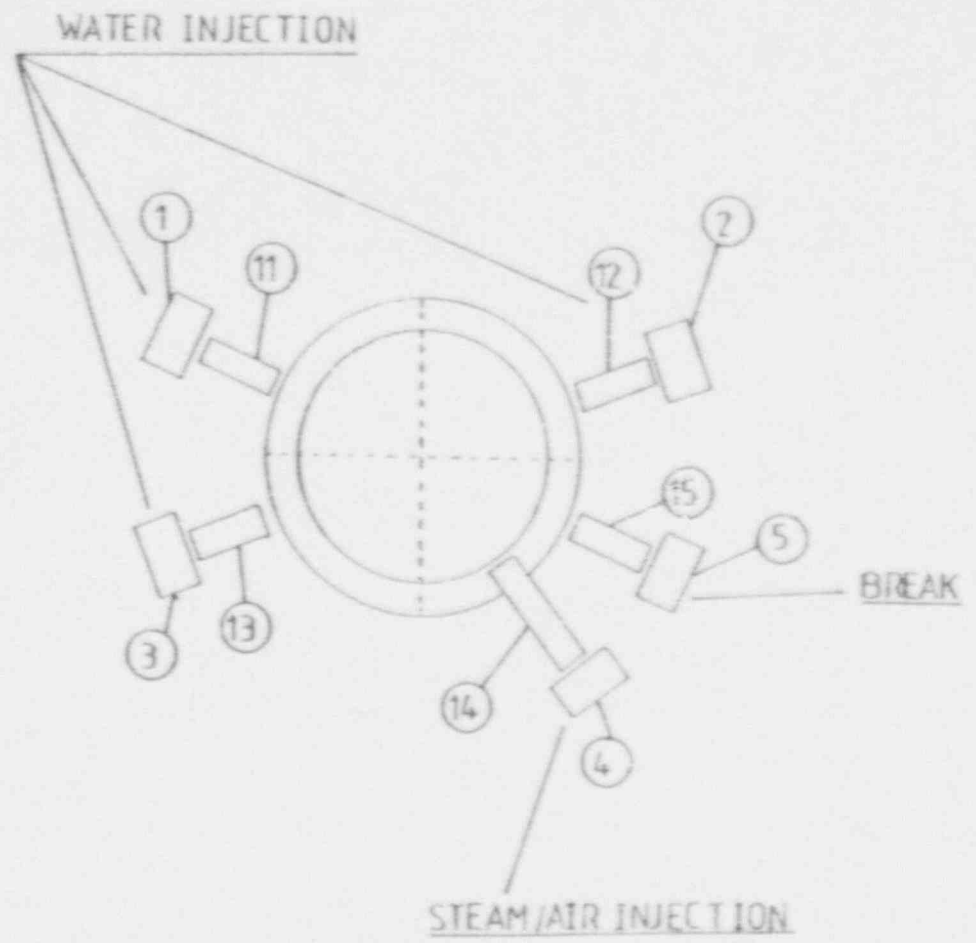
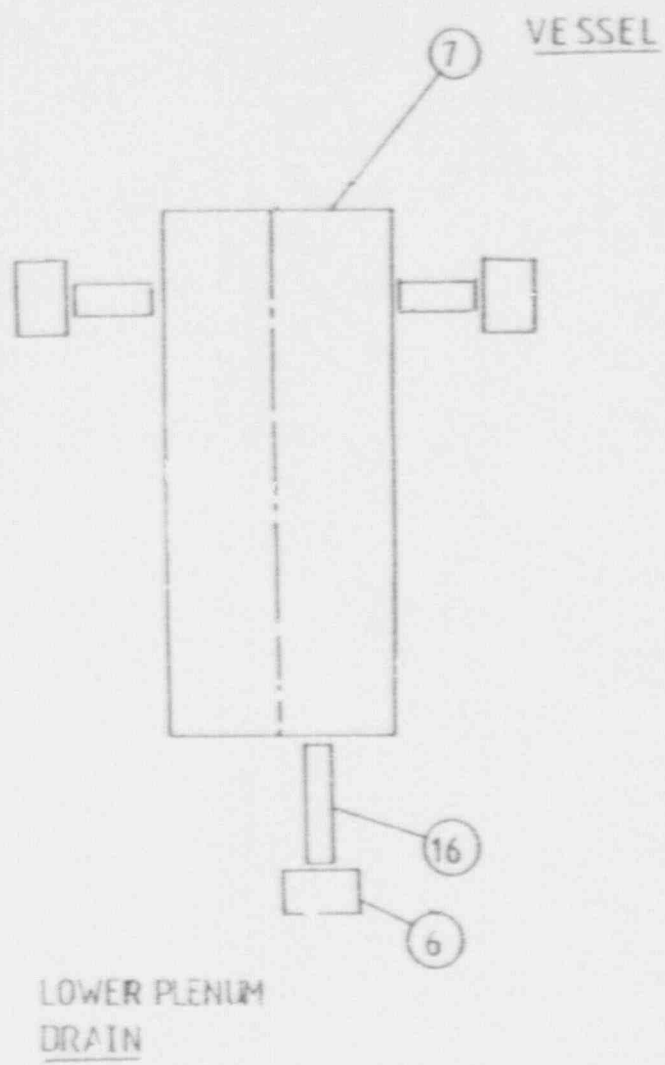


FIG. 1.3 NODALISATION SCHEME FOR REFILL RIG

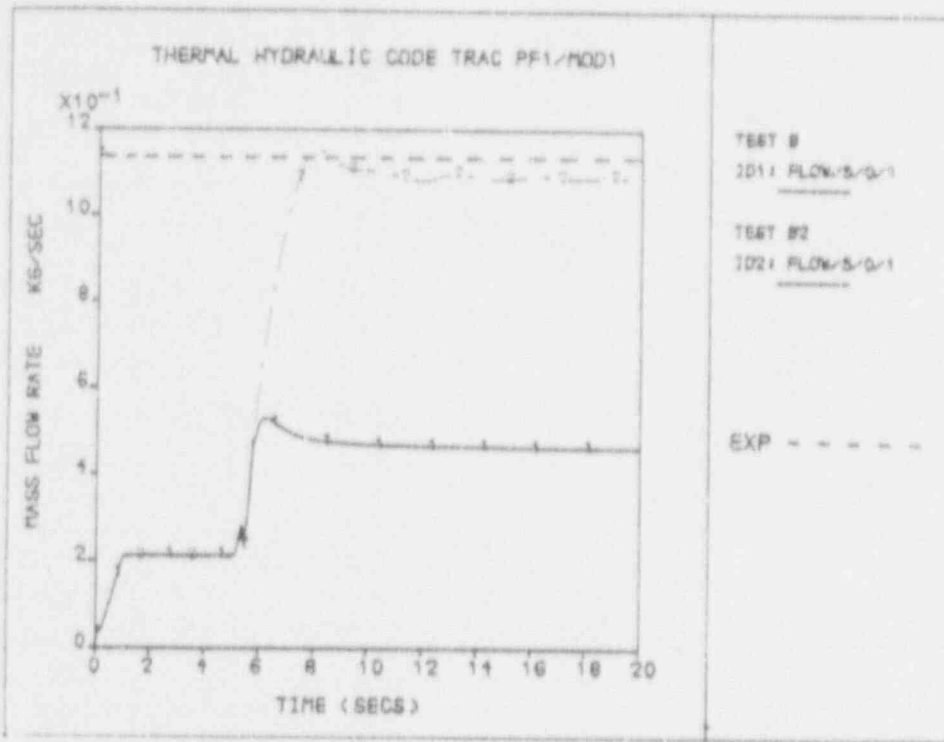


FIG. 2.1 BREAK MASS FLOWRATES FOR TEST B ($D_h=0.038$ M) AND TEST B2 ($D_h=0.019$ M)

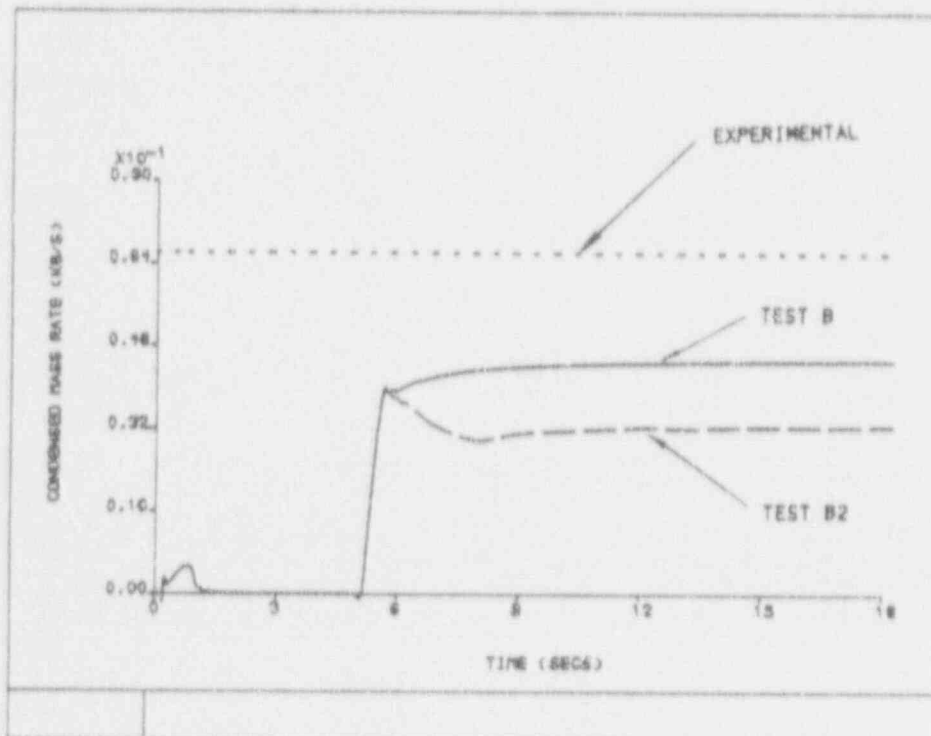


FIG. 2.2 STEAM CONDENSATION RATES FOR TEST B ($D_h=0.038$ M) AND TEST B2 ($D_h=0.019$ M)

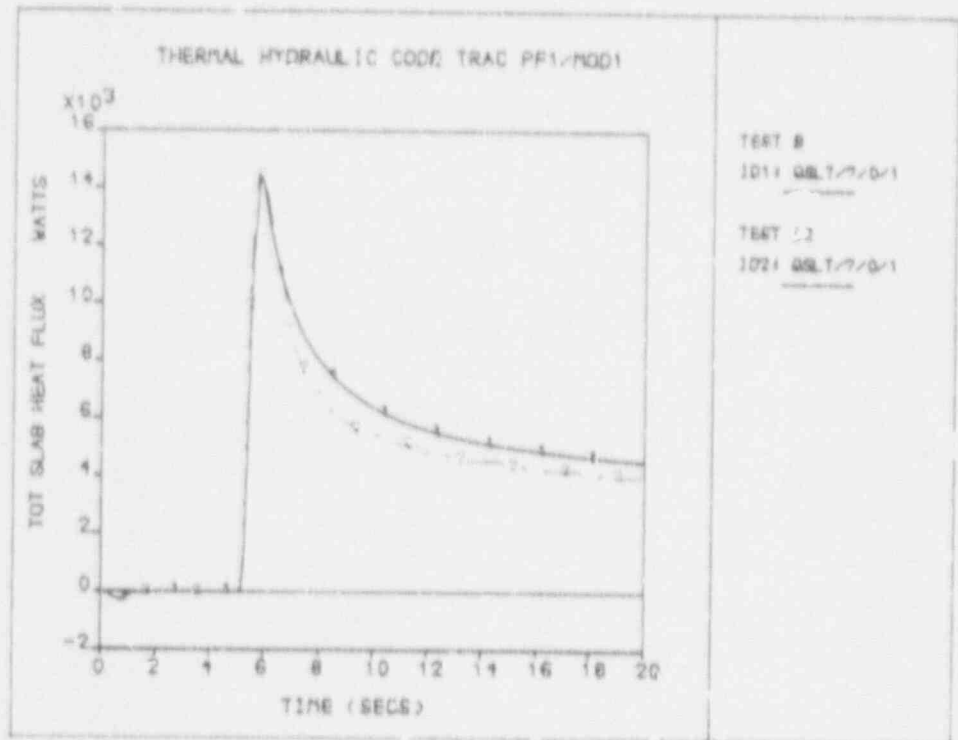


FIG. 2.3 TOTAL WALL HEAT TRANSFER FOR TEST B ($D_h=0.038$ M) AND TEST B2 ($D_h=0.019$ M)

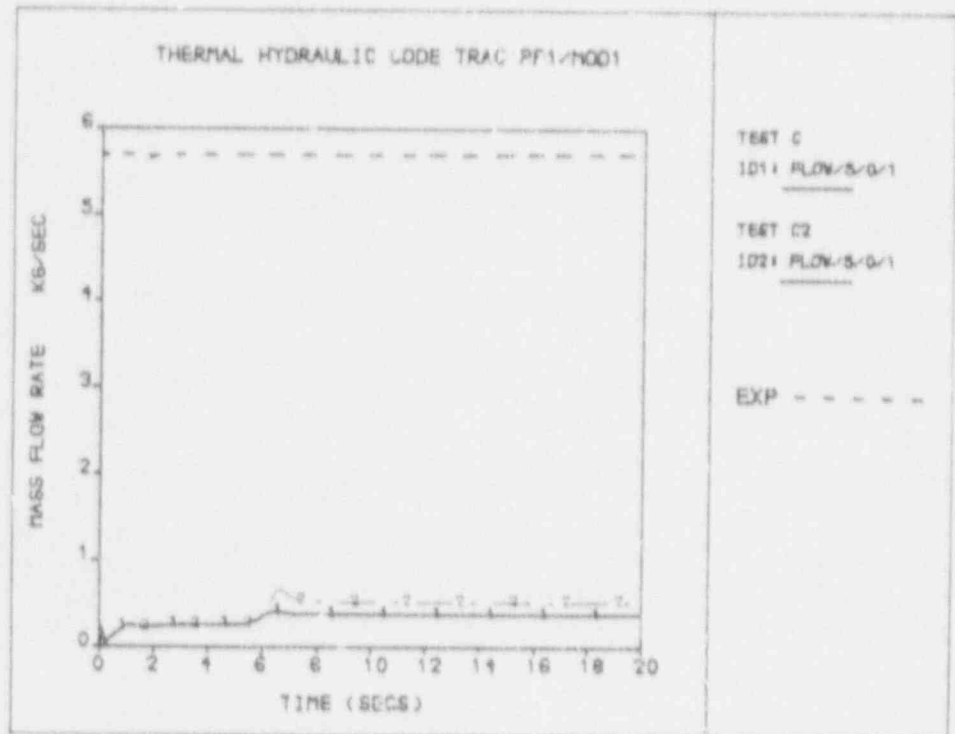


FIG. 2.4 BREAK MASS FLOWRATES FOR TEST C ($D_h=0.038$ M) AND TEST C2 ($D_h=0.019$ M)

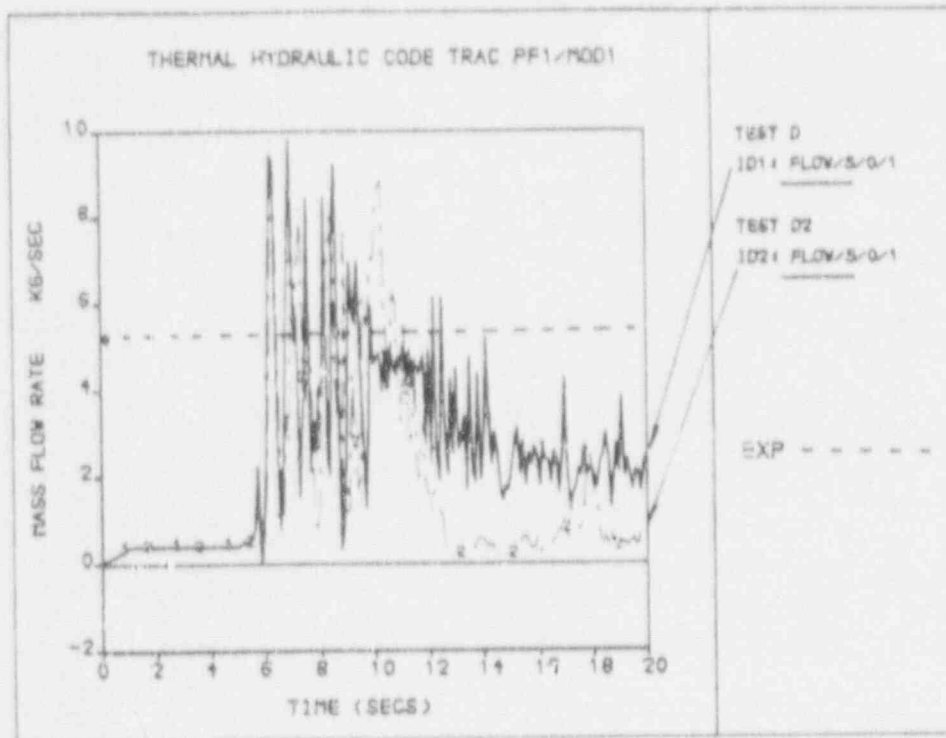


FIG. 2.5 BREAK MASS FLOWRATES FOR TEST D ($D_h=0.038$ M) AND TEST D2 ($D_h=0.019$ M)

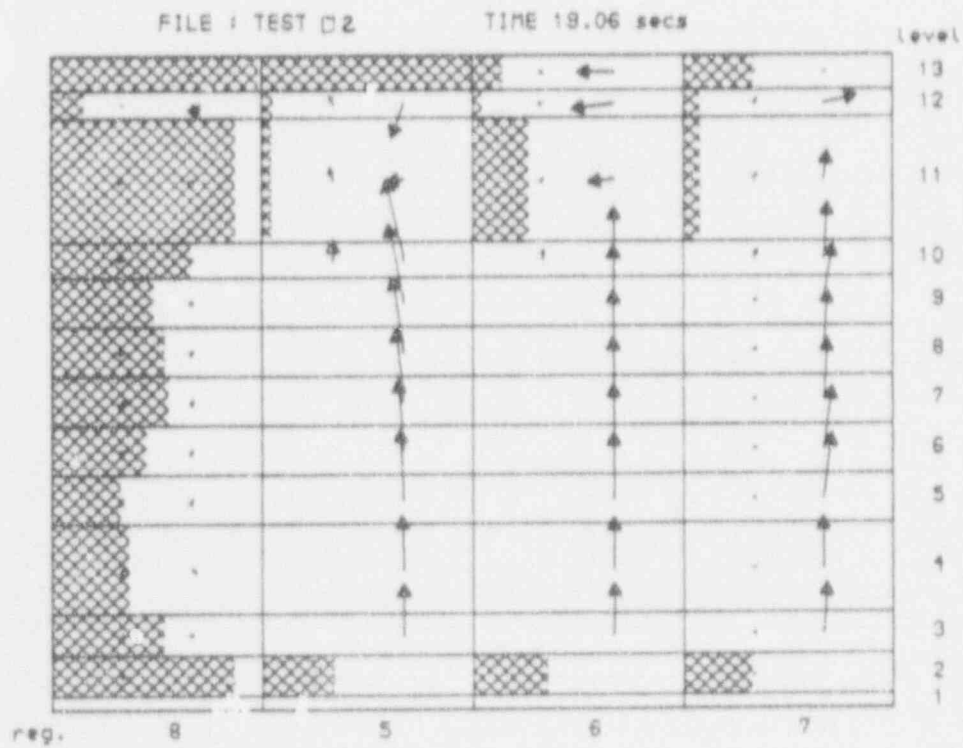
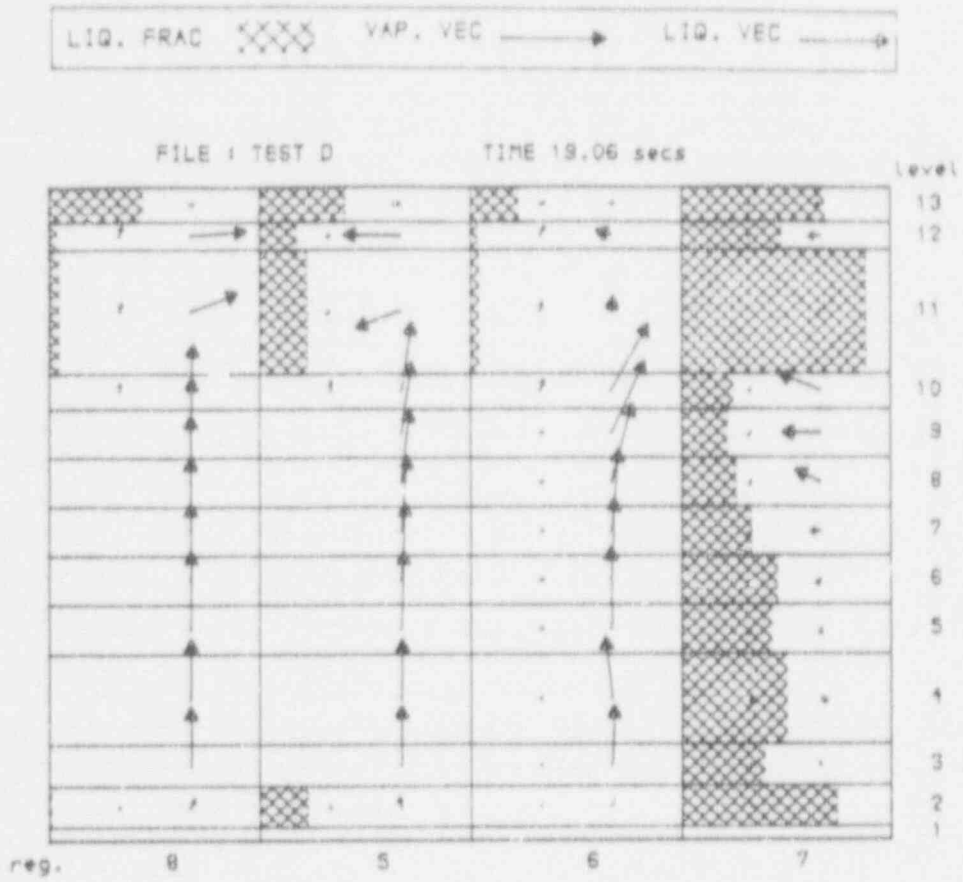


FIG. 2.6 VELOCITY VECTOR PLOT AND LIQUID FRACTION DISTRIBUTION FOR TEST D ($D_h=0.038$ M) AND TEST D2 ($D_h=0.019$ M)

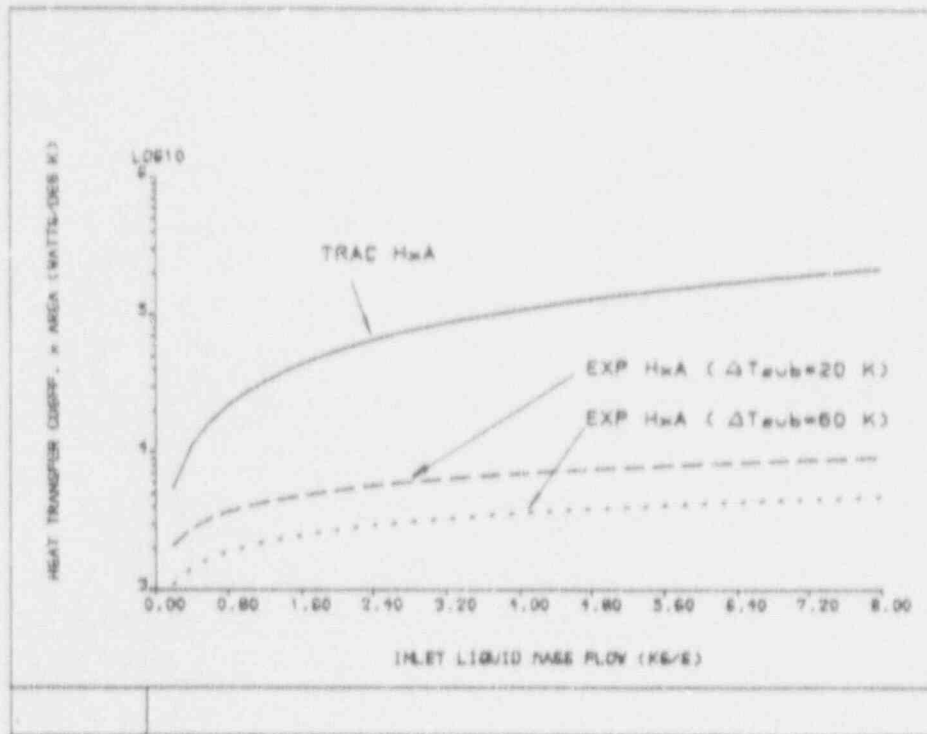


FIG. 3.1 INTERFACIAL HEAT TRANSFER RATES: COMPARISON BETWEEN TRAC AND EXPERIMENTALLY DERIVED VALUES

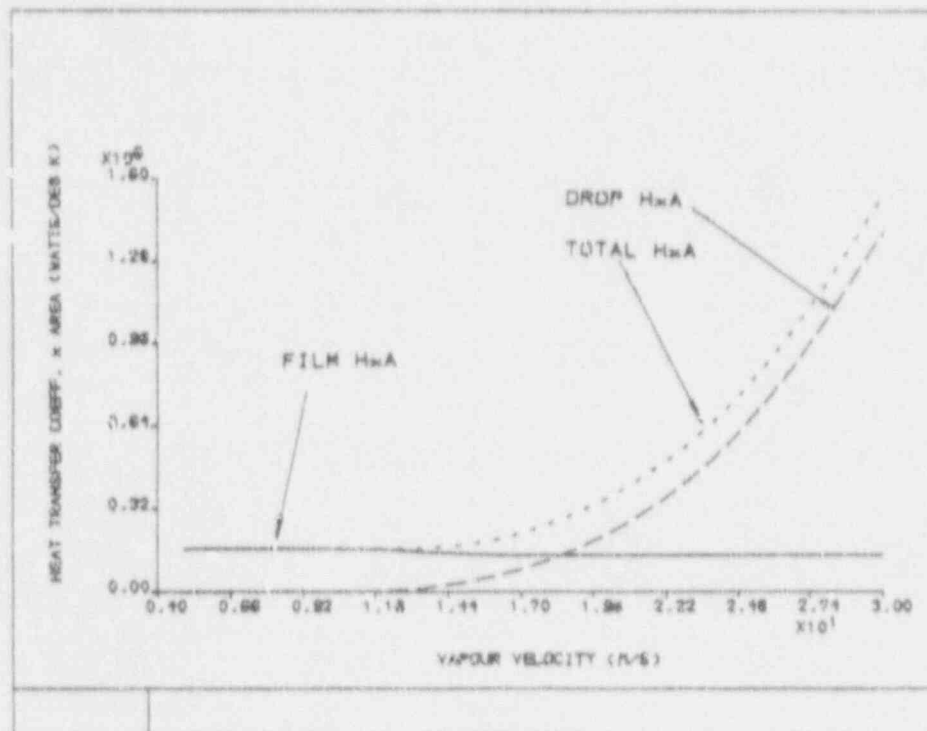


FIG. 3.2 INTERFACIAL HEAT TRANSFER RATES FOR TRAC FILM AND DROP MODELS

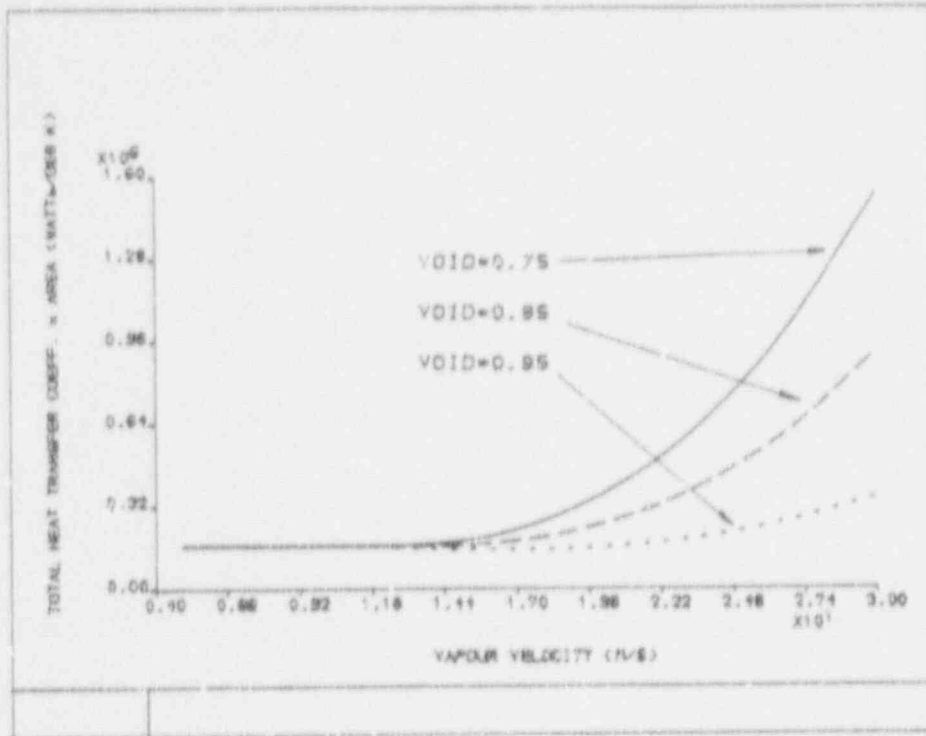


FIG. 3.3 ANNULAR-MIST INTERFACIAL HEAT TRANSFER RATES FOR VARIATION IN VOID FRACTION

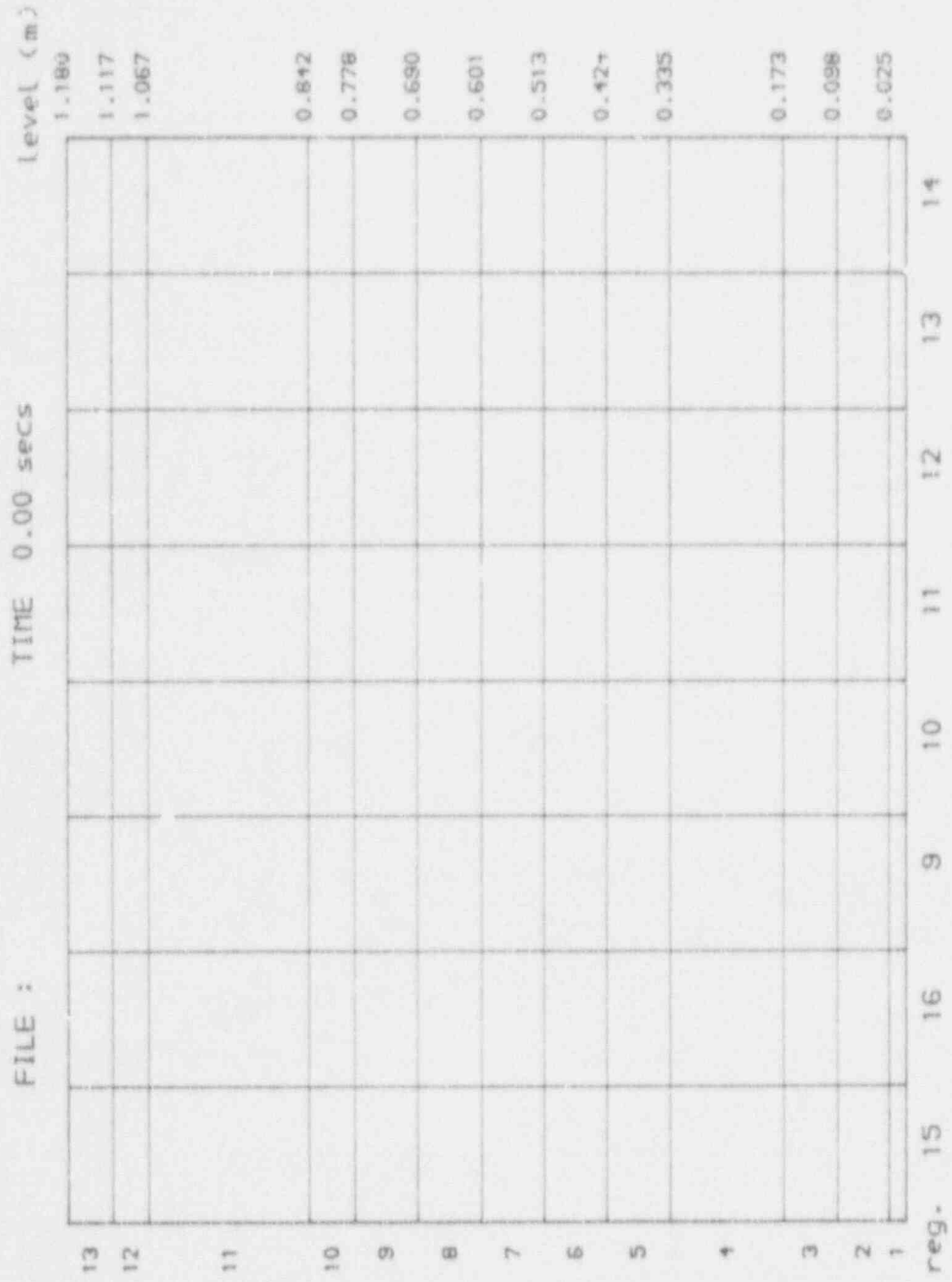


FIG. 4.1 DOWNCOMER NODALISATION FOR 13x8x2 GRID

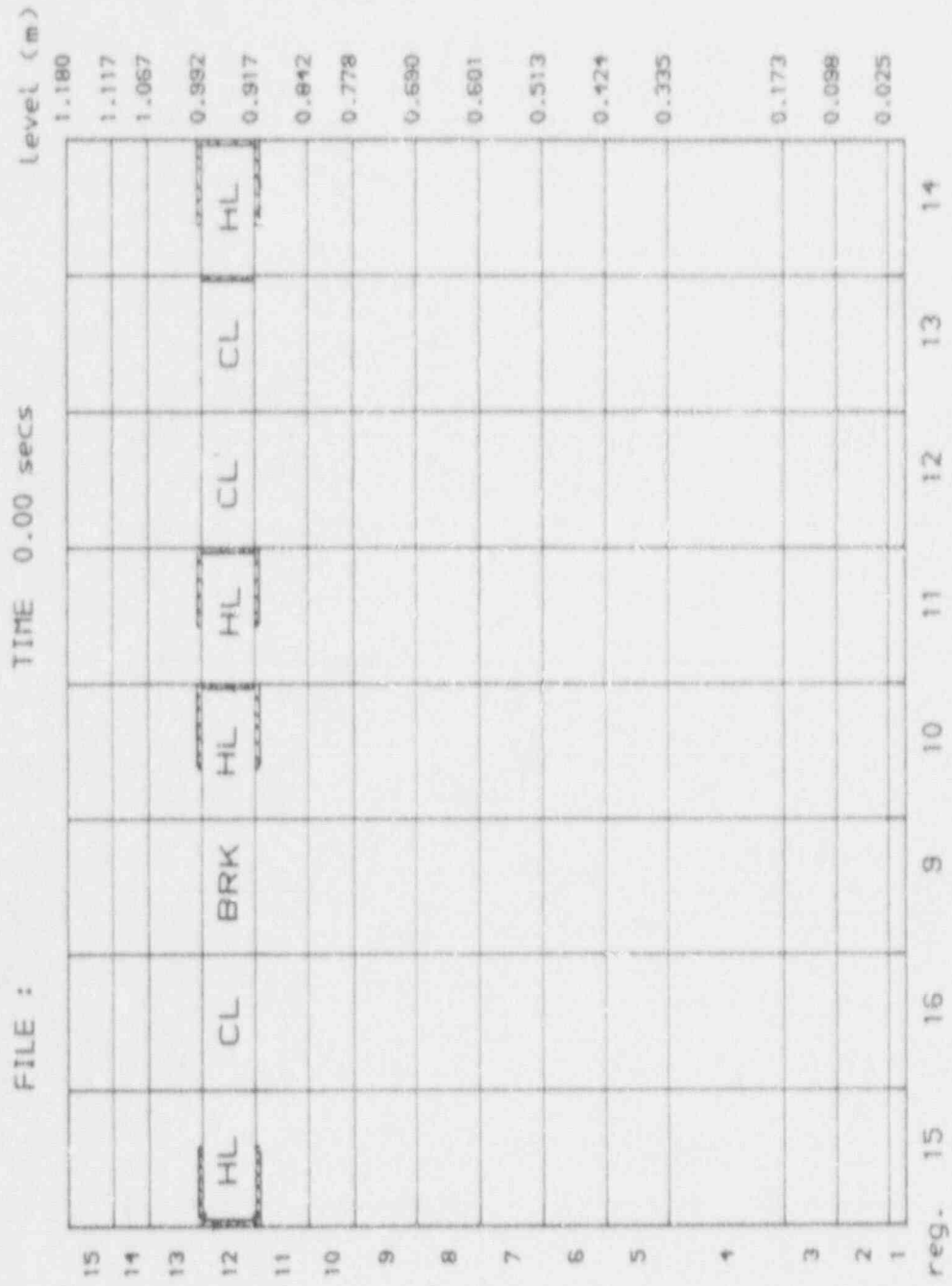


FIG. 4.2 DOWN-COMER REGOALISATION FOR 15x8x2 GRID AND FLOW AREA BLOCKAGES FOR TEST 57 58 AND 59

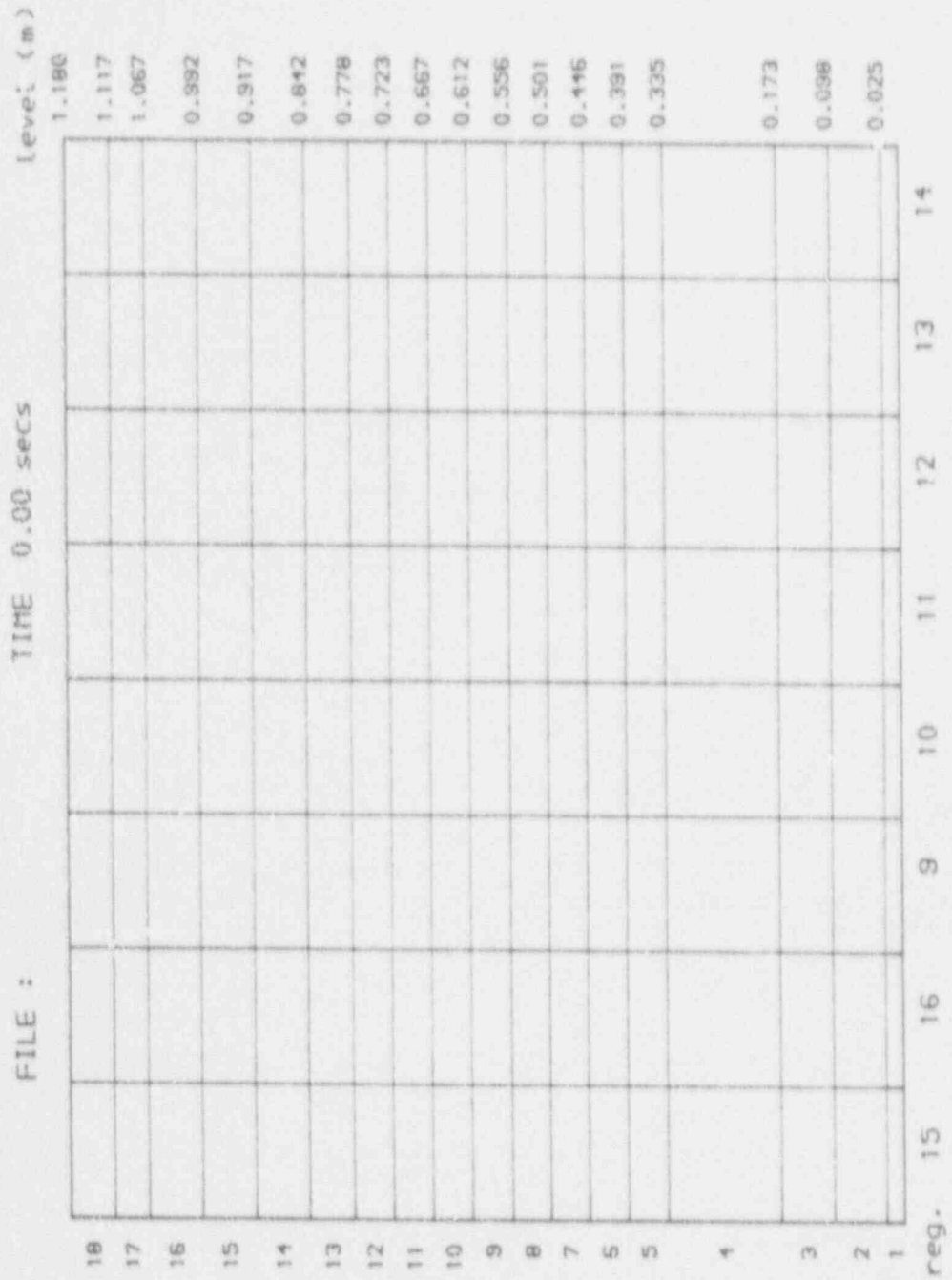


FIG. 4.3 DOWNCOMER NODALISATION FOR 18x8x2 GRID

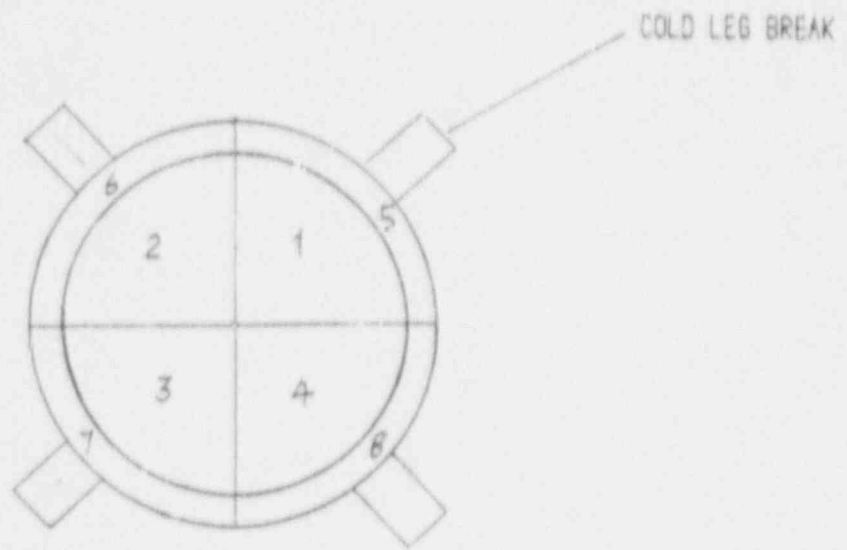


FIG. 4.4A ECC INJECTION POINTS AND COLD LEG BREAK POSITIONS FOR FOUR SEGMENT GRID CALCULATIONS

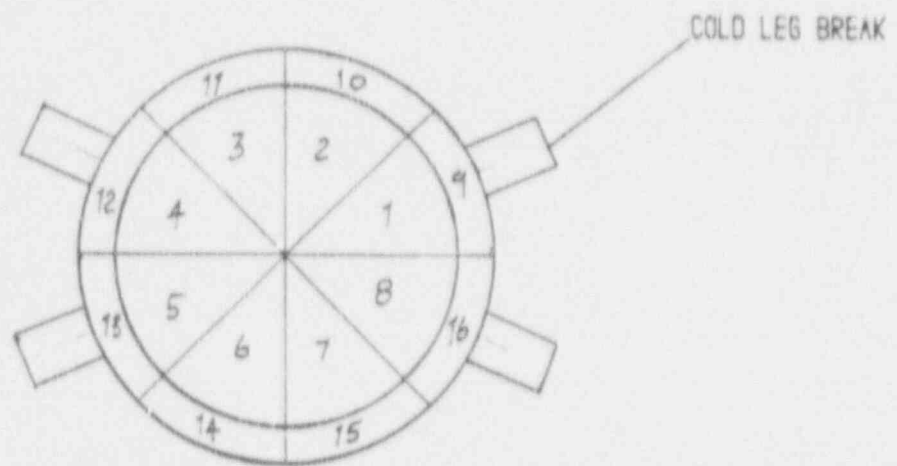


FIG. 4.4B ECC INJECTION POINTS AND COLD LEG BREAK POSITIONS FOR EIGHT SEGMENT GRID CALCULATIONS

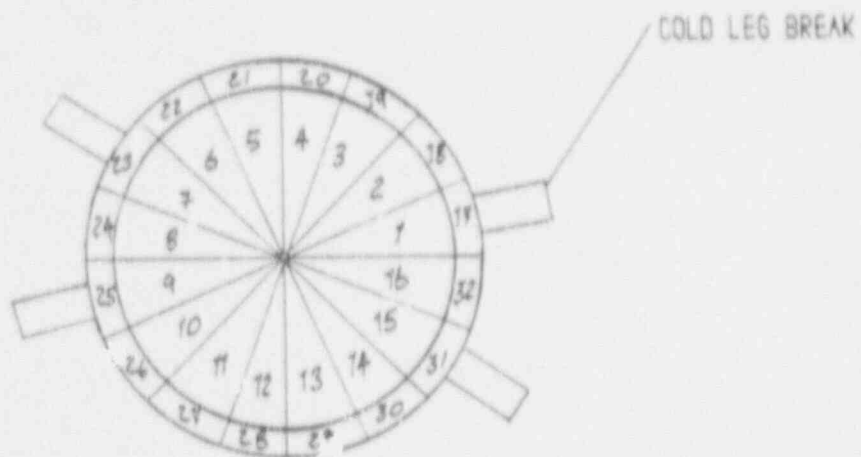


FIG. 4.4C ECC INJECTION POINTS AND COLD LEG BREAK POSITIONS FOR SIXTEEN SEGMENT GRID CALCULATIONS

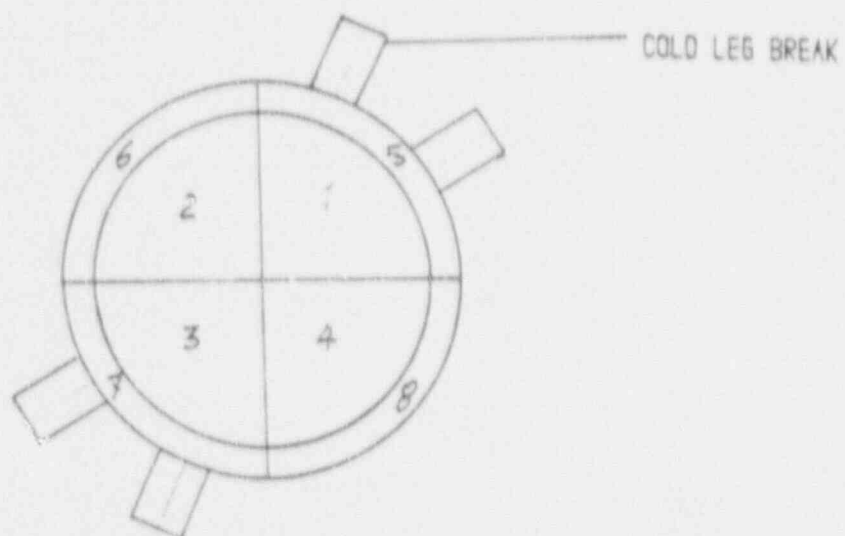


FIG. 4.5 ECC INJECTION POINTS AND COLD LEG BREAK POSITIONS FOR TEST 2.5

FILE : TEST S1 TIME 4.54 secs

Level	8	5	6	7
13	0.0 16.3 3.1 22.1	0.0 -16.3 -6.8 -22.1	0.0 -0.3 3.1 -6.0	0.0 5.3 2.1 6.0
11	0.0 16.8	-16.3 -16.8	5.3 -6.0	1.2 6.0
10	16.0 7.8	30.3 -7.8	16.0 -3.0	16.4 3.0
9	20.0 5.6	27.3 -5.0	20.0 -2.2	17.6 2.2
8	20.7 2.8	24.6 -2.8	20.7 -1.4	19.8 1.4
7	21.1 1.6	23.1 -1.6	21.1 -0.8	19.3 0.8
6	21.3 2.8	22.3 -0.8	21.3 -0.4	20.0 0.4
5	21.4 0.2	21.8 -0.2	21.4 -0.1	20.2 0.1
4	16.2 0.1	16.3 -0.1	16.2 0.0	15.3 -0.0
3	16.3 -0.2	16.1 0.2	16.3 0.3	15.3 -0.3
2	4.7 -0.8	4.5 0.8	4.7 -1.4	1.6 1.4
1				

reg. 8 5 6 7 velocity components v_x v_y v_z

FIG. 4.6 CELL EDGE AXIAL (v_x) AND CIRCUMFERENTIAL (v_y) VAPOUR VELOCITY COMPONENTS FOR TEST S1 (13x4x2 GRID)

FILE : TEST S2 TIME 4.51 secs Level

Level	15	16	9	10	11	12	13	14
13	0.0	0.0	0.0	0.0	0.0	0.0	0.0	0.0
12	14.1	0.0	-16.6	-10.4	2.3	11.4	5.4	-6.2
11	0.0	-2.3	-11.3	2.2	0.2	3.8	-1.3	-6.7
10	17.3	16.3	-23.6	-14.5	-8.2	8.5	6.1	11.0
9	10.8	-2.8	-22.8	0.3	7.6	6.0	-1.1	-4.8
8	15.8	20.5	-28.2	-17.7	-11.4	-7.8	1.5	12.4
7	20.7	20.8	34.5	26.0	21.5	17.2	15.3	13.3
6	6.1	10.2	-7.1	-8.5	-6.5	-1.4	-0.8	5.8
5	21.1	22.2	27.6	20.5	22.2	18.0	16.7	12.8
4	9.1	1.7	-1.5	-5.3	-4.8	-3.0	0.2	3.8
3	21.7	21.8	24.3	23.4	22.5	18.0	18.4	17.8
2	3.2	2.5	-0.5	-3.0	-3.0	-1.8	0.1	2.3
1	22.2	21.9	22.7	22.1	22.5	18.6	18.5	18.1
	1.8	1.3	-0.2	-1.7	-1.7	-1.1	0.0	1.3
	22.5	21.2	21.8	21.4	22.5	18.8	20.1	19.8
	1.2	0.7	-0.1	-1.0	-0.8	-0.6	-0.6	0.6
	22.8	20.8	21.4	20.5	22.5	20.1	20.4	20.1
	1.1	0.5	-0.1	-1.0	-0.0	-0.3	-0.1	-0.2
	17.8	16.5	16.8	16.4	17.4	15.0	15.5	15.1
	0.6	0.4	-0.4	-0.6	0.1	0.2	-0.3	-0.1
	18.2	18.3	15.1	15.2	17.8	15.1	15.0	15.2
	0.8	1.6	-2.1	-1.2	1.2	2.1	-1.6	-0.8
	3.0	-5.1	-0.3	-0.1	3.4	-5.9	-5.2	-5.1
	-8.0	-0.5	0.8	0.3	-8.3	-0.8	0.5	7.8

reg. 15 16 9 10 11 12 13 14
velocity components v_r v_θ

FIG. 4.7 CELL EDGE AXIAL (V_r) AND CIRCUMFERENTIAL (V_θ) VAPOUR VELOCITY COMPONENTS FOR TEST S2 (13*8*2 GRID)

FILE : TEST S3 TIME 4.51 secs

Level	29	30	31	32	17	18	19	20	21	22	23	24	25	26	27	28	
13	15.2	17.0	20.8	25.7	25.8	17.3	6.7	-0.8	0.0	0.0	0.0	0.0	0.0	0.0	0.0	0.0	
12	-0.1	1.8	3.1	4.5	0.0	-7.2	-9.2	-9.7	-3.1	2.1	2.8	4.5	1.6	1.8	2.9	3.7	
	18.0	18.8	24.4	31.0	32.0	21.7	8.6	-2.0	-8.3	-1.4	1.3	5.8	0.8	0.8	11.7	18.3	
11	-0.8	4.0	6.4	8.8	9.6	-13.7	-16.4	-13.8	-0.1	4.5	4.4	4.0	2.8	3.5	4.5	6.5	
	20.4	26.1	32.5	40.4	-41.5	-28.8	-16.8	-7.4	-1.8	-6.1	1.8	4.0	6.5	9.2	11.8	14.4	
10	20.6	25.8	31.4	36.5	42.6	27.0	21.4	15.8	13.5	12.1	12.8	13.2	12.0	14.4	17.5	17.5	
	11.8	2.8	10.6	2.4	-15.1	-13.3	-8.4	-1.4	-1.8	0.4	2.4	2.4	5.4	8.4	4	8.8	
9	22.3	26.6	28.7	33.0	25.0	26.8	22.7	18.6	16.6	14.2	14.6	14.8	14.5	15.8	17.3	18.8	
	7.8	7.1	3.6	-3.2	-6.7	-8.2	-8.1	-6.8	-4.3	-2.0	-0.1	1.7	3.4	5.0	6.3	7.2	
8	22.8	25.8	25.9	25.8	25.3	24.2	22.8	22.1	18.4	16.6	16.6	16.8	16.3	17.6	18.7	18.8	
	4.3	3.4	1.3	-1.2	-3.2	-4.8	-5.4	-4.5	-3.1	-1.6	-0.2	1.1	2.3	3.3	4.1	4.4	
7	22.8	24.8	23.6	23.2	23.0	22.6	22.2	23.0	20.8	18.2	18.2	18.2	17.6	18.7	18.5	20.1	
	2.3	1.8	0.8	-0.5	-1.6	-2.5	-3.1	-2.7	-2.0	-1.1	-0.2	0.6	1.4	2.0	2.4	2.4	
6	22.8	24.2	22.3	21.8	21.8	21.6	21.7	23.3	21.7	18.1	18.1	18.1	18.4	18.4	18.8	20.1	
	1.2	1.1	0.5	-0.2	-0.6	-1.5	-1.8	-1.5	-1.0	-0.6	-0.1	0.4	0.8	1.1	1.2	1.2	
5	22.8	24.1	21.6	21.2	21.1	21.0	21.3	23.6	22.2	18.6	18.7	18.6	18.6	18.7	20.0	20.1	
	0.5	1.3	0.8	-0.0	-0.6	-1.1	-1.7	-0.7	0.0	-0.1	0.1	0.4	0.2	0.4	0.4	-0.0	
4	17.7	18.8	18.8	15.5	15.5	15.4	1.7	18.6	17.4	14.7	15.0	15.0	14.1	15.1	15.1	14.8	
	0.6	0.7	0.4	0.1	-0.3	-0.6	-0.8	-0.7	-0.2	0.0	0.1	0.0	0.2	0.1	0.1	0.2	
3	18.2	18.0	18.2	14.8	14.8	14.8	15.1	18.0	18.1	15.1	15.3	14.8	14.4	14.8	15.0	15.0	
	1.8	2.1	0.7	0.3	-0.3	-0.7	-2.1	-2.1	1.0	1.8	0.5	-1.0	1.0	-0.5	-1.8	-1.0	
2	8.0	8.7	-4.8	-4.1	-3.8	-4.0	-4.8	3.8	4.8	-4.6	-4.6	-4.7	-2.8	-4.6	-4.6	-4.5	
	3.5	-8.2	-0.8	0.1	-0.1	0.8	8.2	-3.7	-7.0	0.8	1.3	3.0	-3.0	-1.1	-0.6	6.8	
1	reg.	29	30	31	32	17	18	19	20	21	22	23	24	25	26	27	28

velocity components
vz vt

FIG. 4.8 CELL EDGE AXIAL (Vz) AND CIRCUMFERENTIAL (Vt) VAPOUR VELOCITY COMPONENTS FOR TEST S3 (13x16x2 GRID)

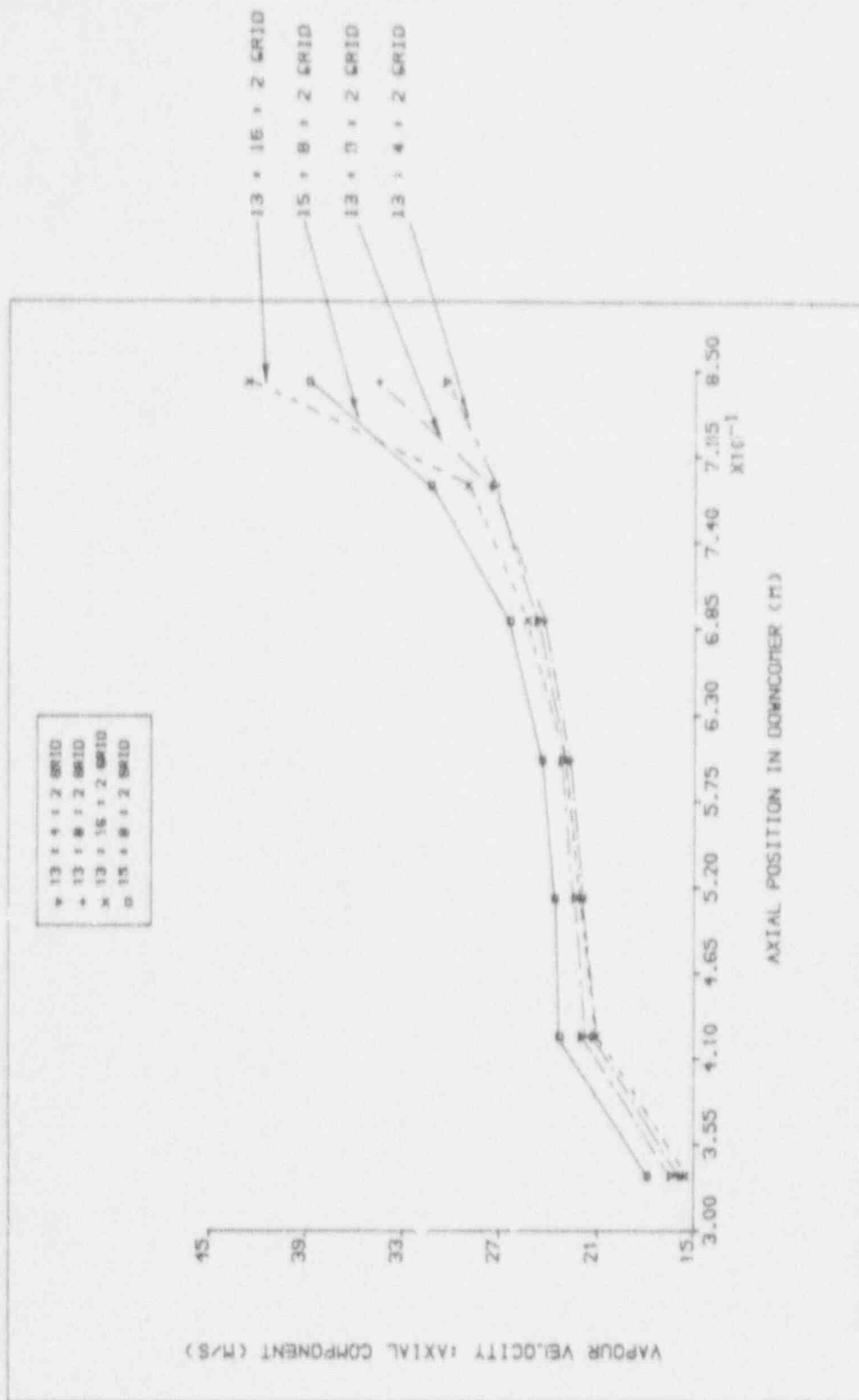


FIG. 4.9 VAPOUR VELOCITY AXIAL COMPONENT IN DOWNCOMER BELOW THE BREAK CELL FOR VARIOUS GRIDS

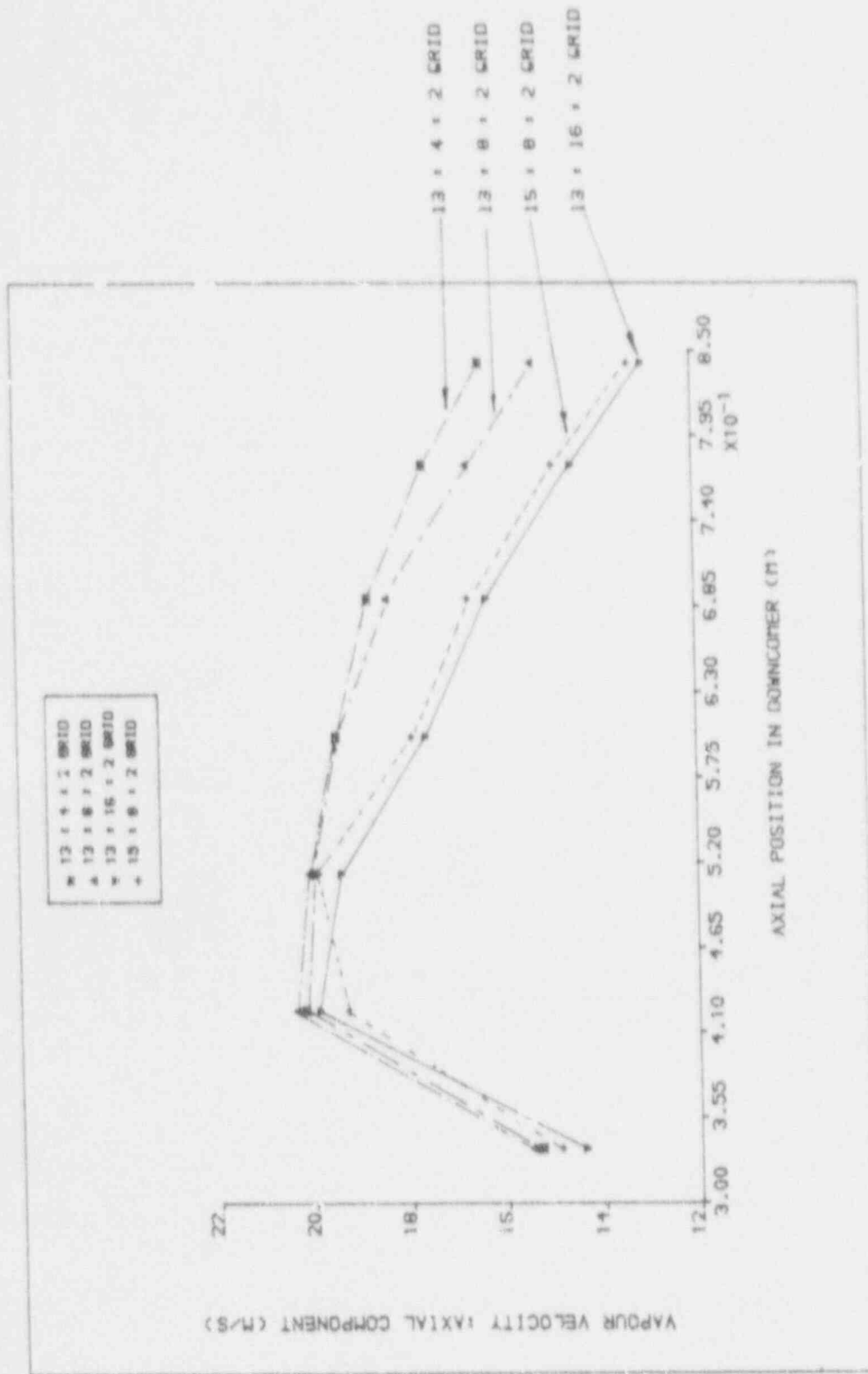


FIG. 4.10 VAPOUR VELOCITY AXIAL COMPONENT IN DOWNCOMER SECTOR FURTHEST FROM BREAK FOR VARIOUS GRIDS

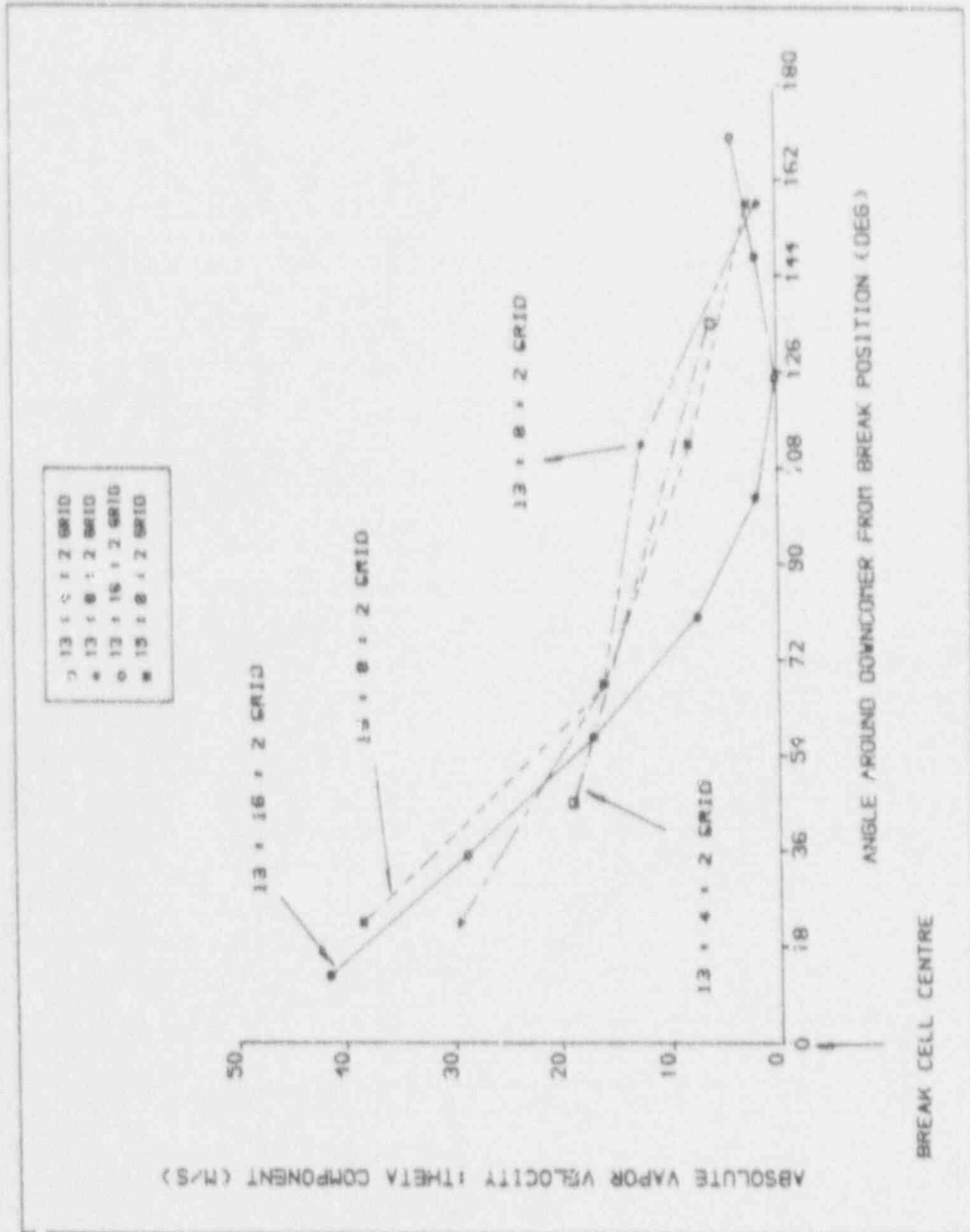


FIG. 4.11 VAPOUR VELOCITY THETA COMPONENT AROUND DOWNCOMER AT THE BREAK LEVEL FOR VARIOUS GRIDS

FILE : TEST S5 TIME 4.50 secs Level

Level	15	16	9	10	11	12	13	14
15	0.0	0.0	0.0	0.0	0.0	0.0	0.0	2.0
14	12.0	8.8	-11.1	-10.6	-4.6	-2.1	2.8	6.0
13	12.7	-0.8	-8.2	-10.9	-8.6	-1.6	7.2	7.1
12	14.2	-15.4	-15.4	-11.9	-6.6	-1.6	2.1	6.0
11	4.6	-0.5	-18.2	1.3	4.1	2.2	3.4	2.6
10	14.0	24.4	-25.3	-13.8	-7.1	-2.1	2.4	7.4
9	7.6	4.2	-40.8	6.5	7.5	4.8	9.2	1.9
8	16.1	38.4	-38.0	-17.0	-8.4	-2.6	2.5	9.1
7	11.3	1.4	47.9	16.6	11.4	7.2	7.9	7.5
6	13.1	1.4	-20.4	-15.2	-8.6	-2.7	7.3	7.8
5	18.2	17.2	38.8	25.1	18.8	13.4	13.3	13.2
4	5.7	14.0	-8.2	-10.8	-7.0	-2.5	1.8	6.1
3	16.5	25.3	31.3	24.4	20.4	15.2	14.9	14.8
2	6.9	5.1	-4.2	-7.3	-5.5	-2.0	1.3	4.6
1	20.7	22.4	26.4	22.8	21.4	17.1	16.7	16.7
	4.0	2.2	-1.7	-4.2	-3.6	-1.5	1.8	3.0
	21.3	21.5	24.4	21.5	21.9	18.2	17.8	17.8
	2.2	1.0	-6.7	-2.4	-2.2	-1.0	0.4	1.8
	21.7	21.0	23.6	26.7	22.1	18.0	18.8	18.7
	1.3	0.4	-0.2	-1.5	-1.3	-0.7	0.1	0.9
	22.0	20.8	23.3	20.1	22.3	18.4	18.3	18.2
	1.0	-0.2	0.4	-1.2	-0.4	-0.9	-0.1	-0.1
	17.1	16.1	17.8	14.6	17.2	14.2	14.6	14.6
	0.6	-0.1	0.2	-0.4	-0.6	-0.6	-0.3	0.1
	17.6	14.5	18.3	14.1	17.1	14.8	15.0	15.0
	2.0	-1.5	1.3	0.8	-1.8	-1.0	-0.8	-0.1
	4.1	-5.8	6.1	-3.5	4.4	-5.1	-5.8	-5.4
	-13.2	13.3	-10.5	16.3	-7.8	-2.6	0.7	8.6

reg. 15 16 9 10 11 12 13 14
velocity components vx vz

FIG. 4.12 CELL EDGE AXIAL (V_x) AND CIRCUMFERENTIAL (V_θ) VAPOUR VELOCITY COMPONENTS FOR TEST S5 (15.8x2 GRID)

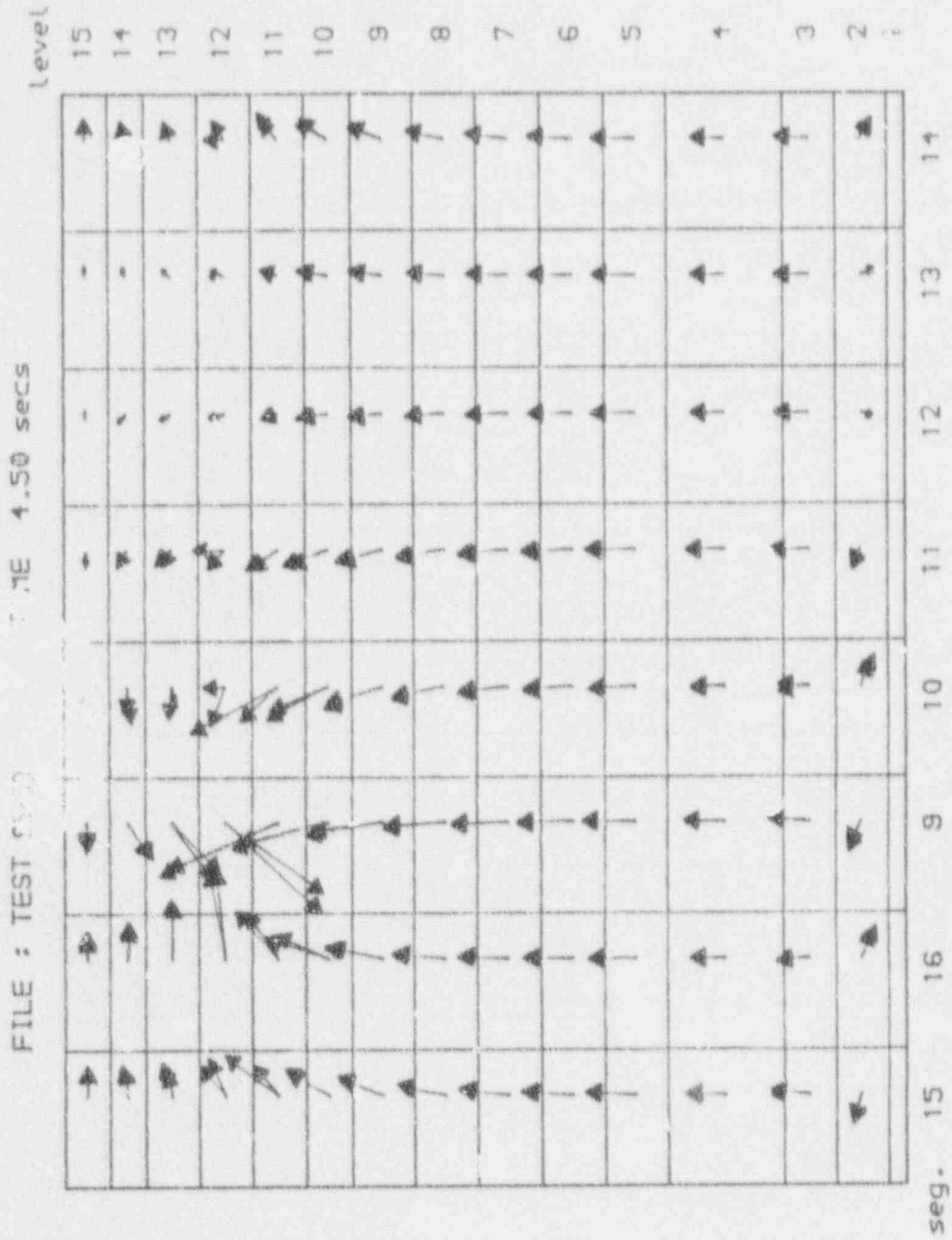


FIG. 4.13 VAPOUR VELOCITY DISTRIBUTIONS FOR TEST 55 (NO FLOW AREA BLOCKAGE, BLACK ARROW) AND 59 (FLOW AREA BLOCKAGE, RED ARROW)

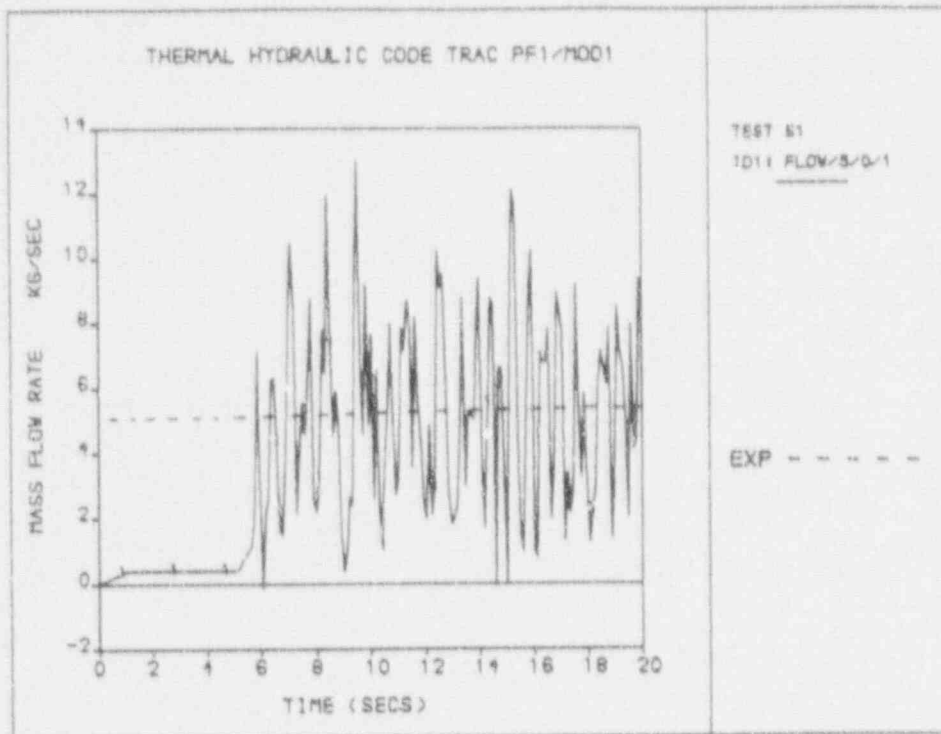


FIG. 4.14 BREAK MASSFLOW FOR TEST S1 (13:4:2 GRID)

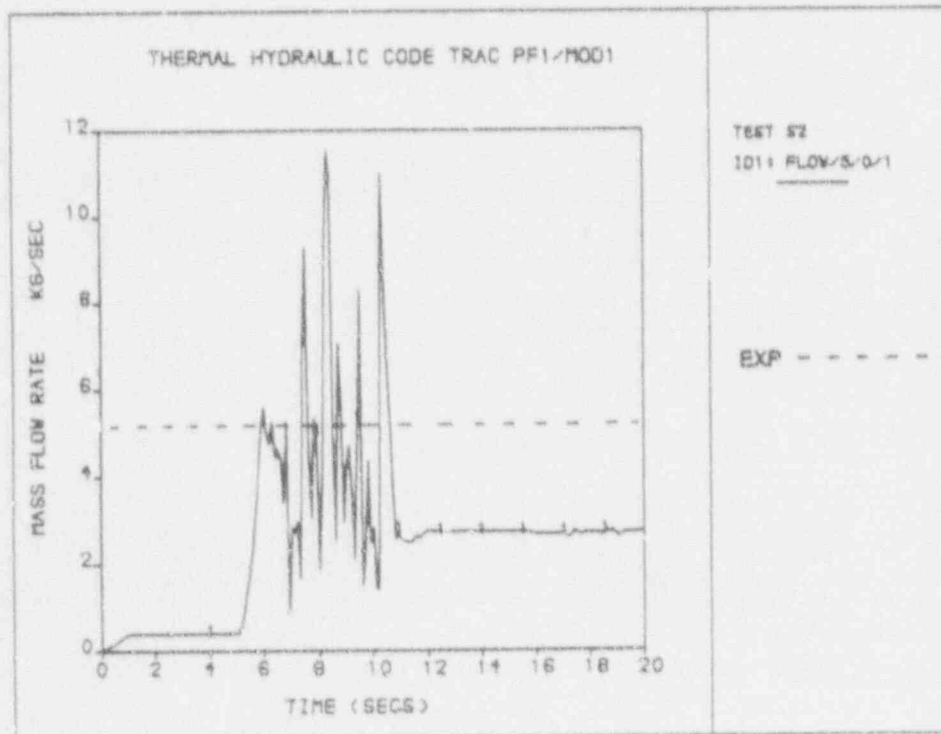


FIG. 4.15 BREAK MASSFLOW FOR TEST S2 (13:8:2 GRID)

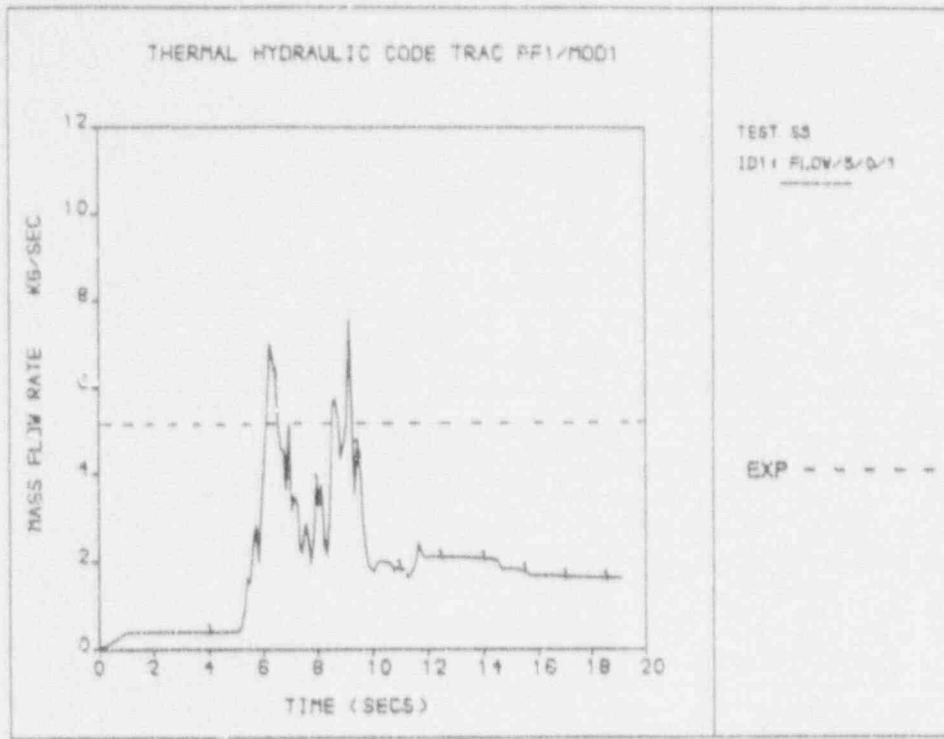


FIG. 4.16 BREAK MASSFLOW FOR TEST S5 (15x8x2 GRID)

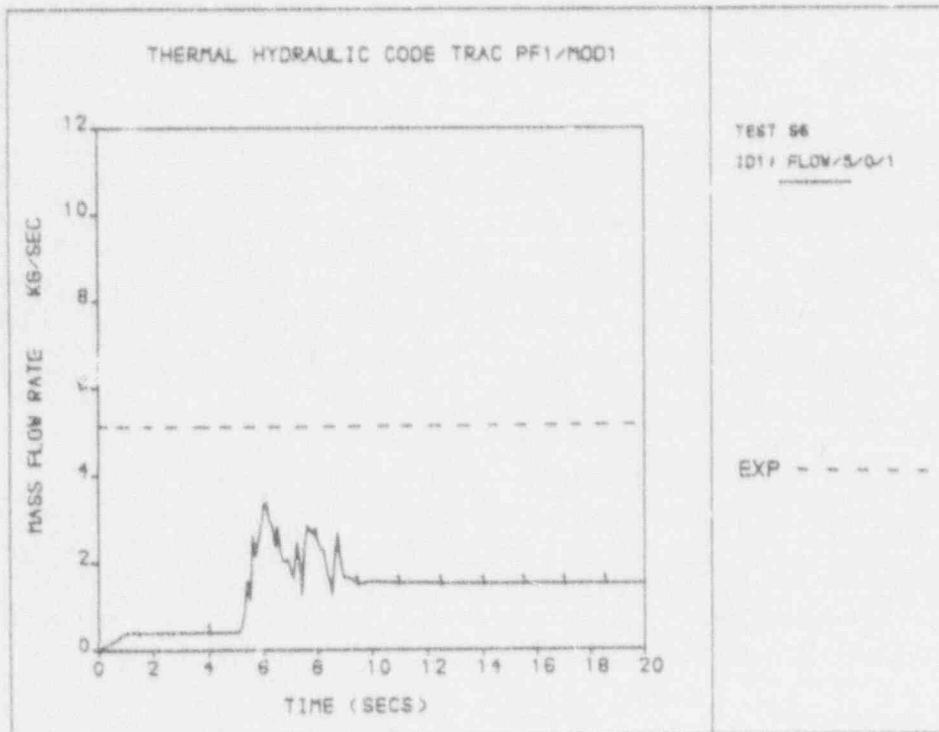


FIG. 4.17 BREAK MASSFLOW FOR TEST S6 (18x8x2 GRID)

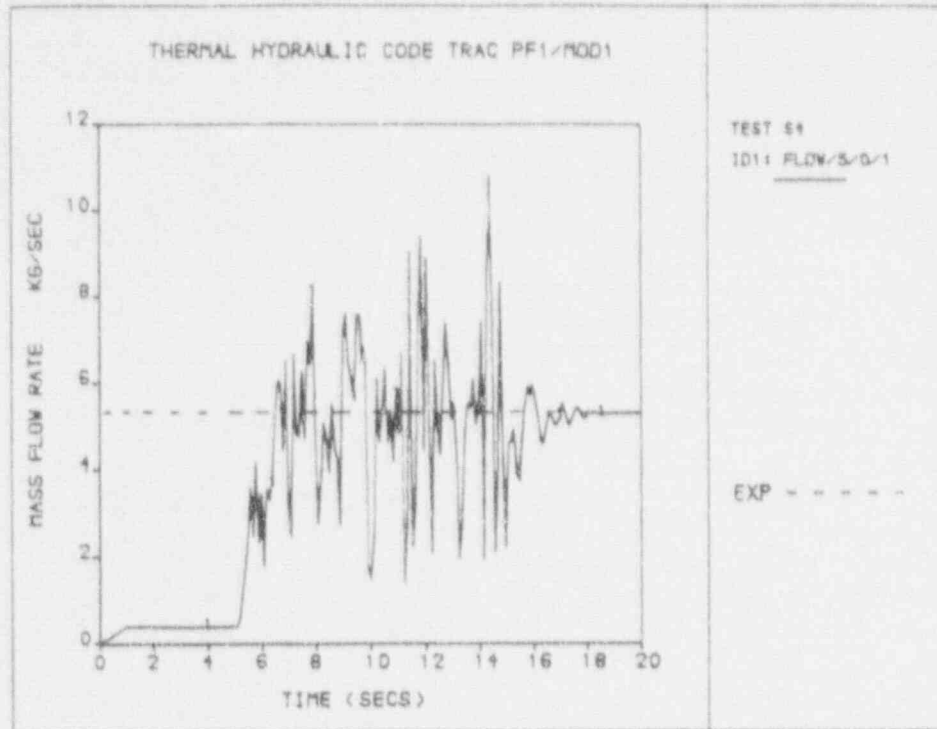


FIG. 4.18 BREAK MASSFLOW FOR TEST S4 (15:4:2 GRID)

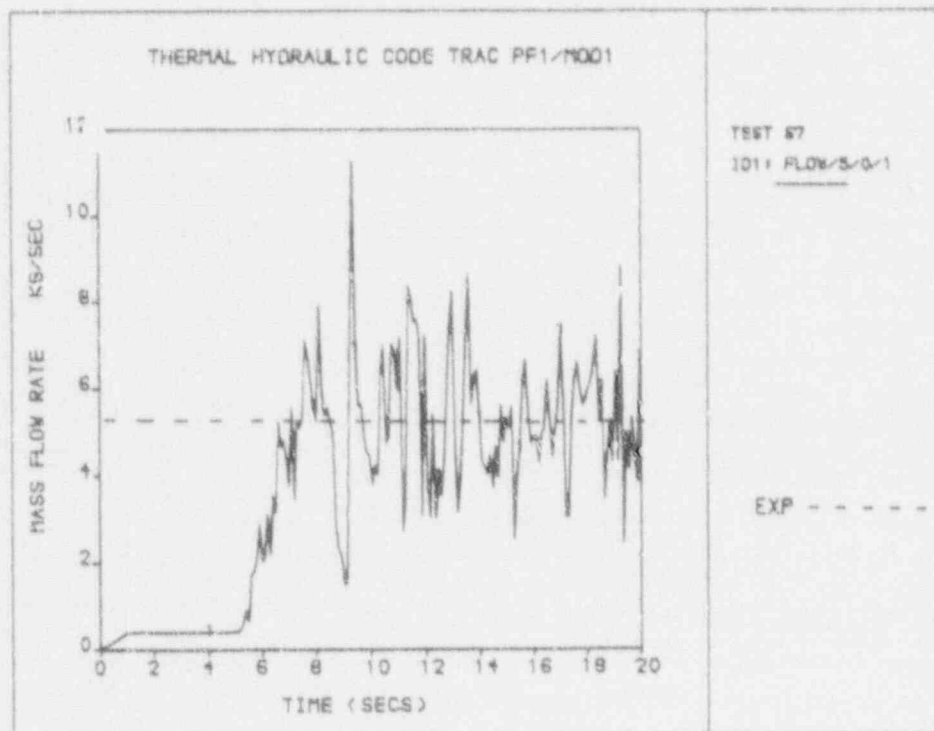




FIG. 4.19 BREAK MASSFLOW FOR TEST S7 (13:4:2 GRID WITH BLOCKAGE)

LIQ. FRAC  VAP. VEC  LIQ. VEC 

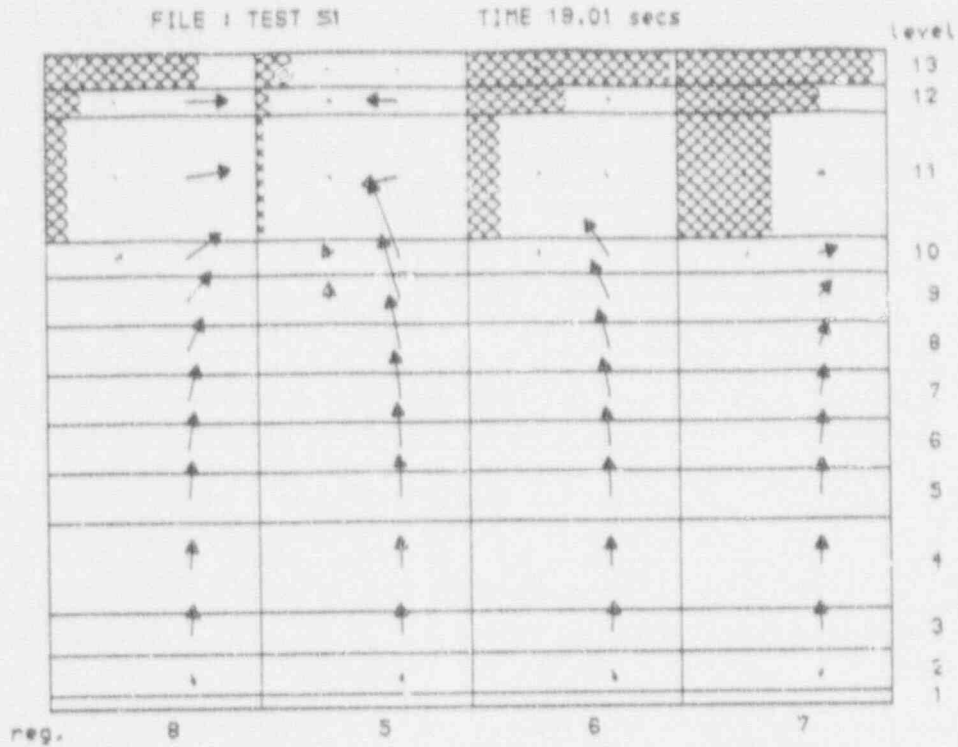


FIG. 4.20 VELOCITY VECTOR AND LIQUID FRACTION DISTRIBUTION FOR TEST S1 (13:4:2 GRID)

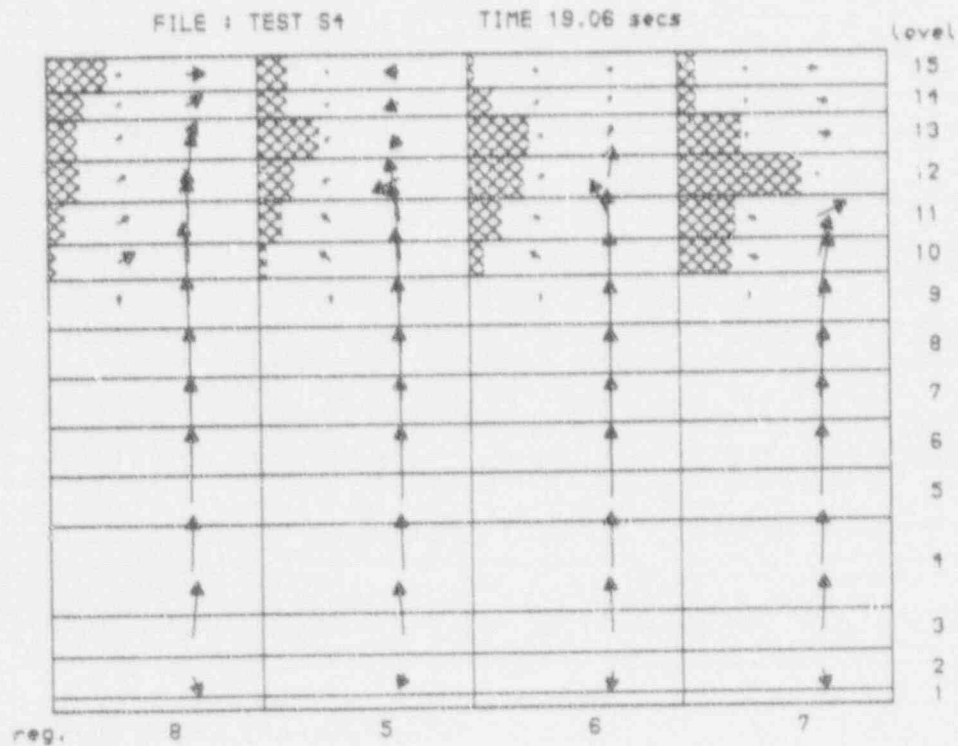


FIG. 4.21 VELOCITY VECTOR AND LIQUID FRACTION DISTRIBUTION FOR TEST S4 (15:4:2 GRID)

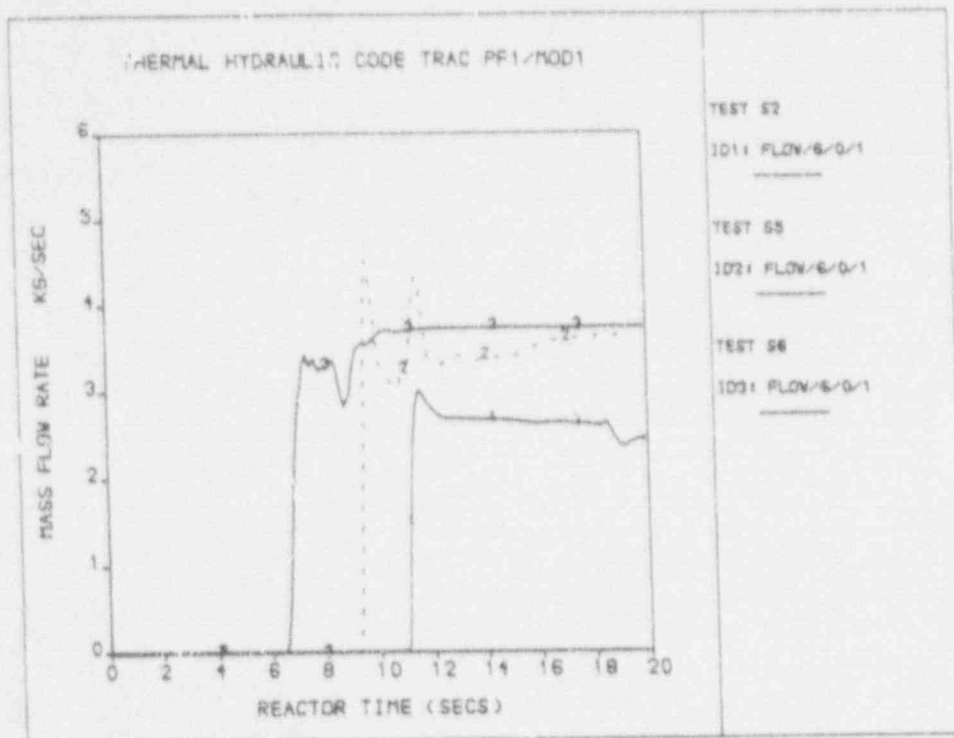


FIG. 4.22 MASS FLOWRATES FROM LOWER PLENUM FOR TESTS S2 (13:8:2 GRID) S5 (15:8:2 GRID) AND S6 (18:8:2 GRID)

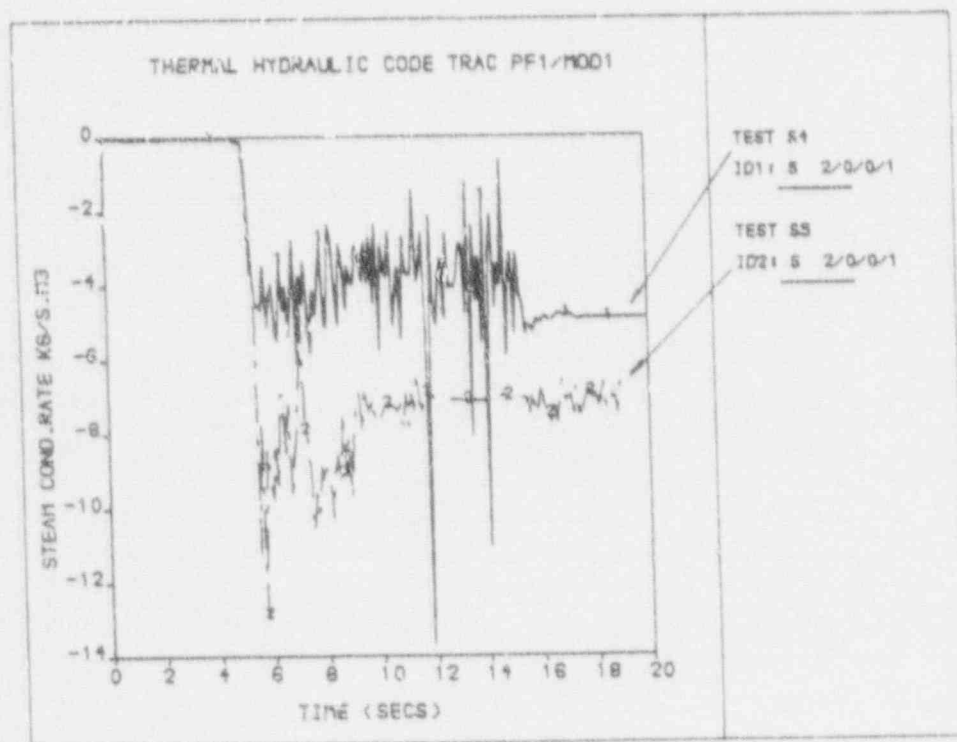


FIG. 4.23 DOWNCOMER STEAM CONDENSATION RATES FOR TEST S4 (15:4:2 GRID) AND S5 (15:8:2 GRID)

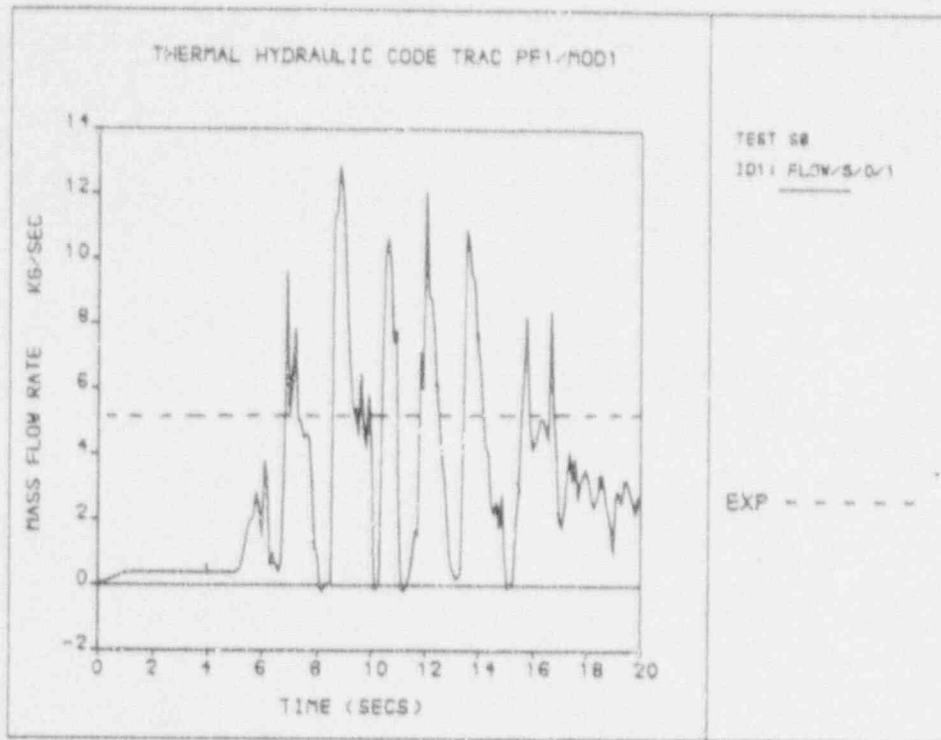


FIG. 4.24 BREAK MASS FLOWRATE FOR TEST S8 (15x8x2 GRID WITH CIRCUMFERENTIAL HOT LEG BLOCKAGE)

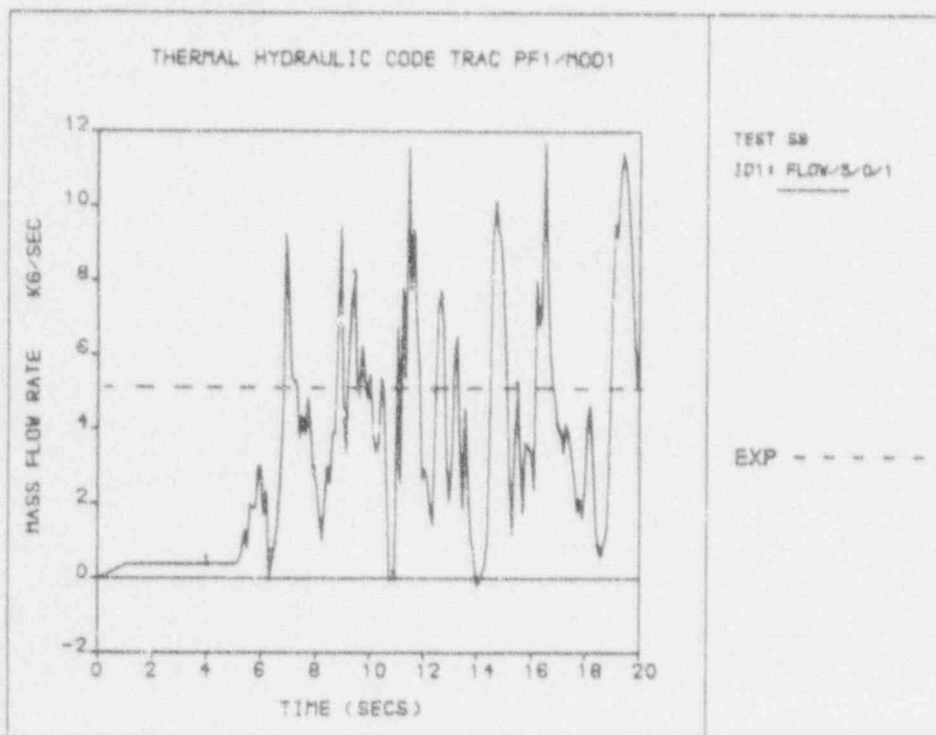


FIG. 4.25 BREAK MASS FLOWRATE FOR TEST S9 (15x8x2 GRID WITH CIRCUMFERENTIAL AND AXIAL HOT LEG BLOCKAGE)

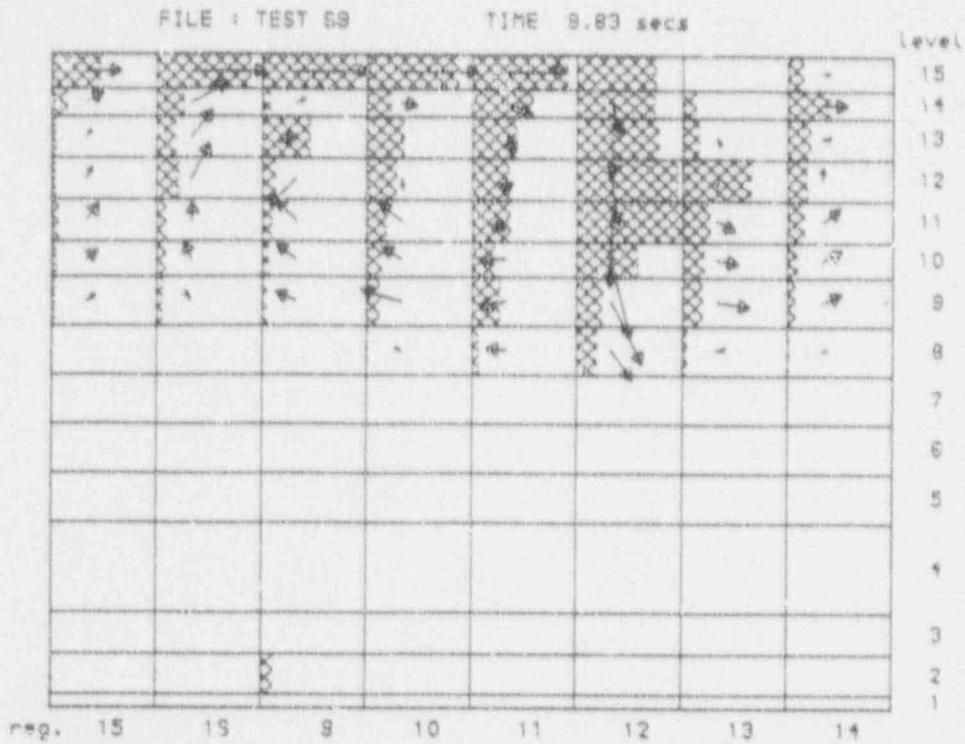


FIG. 4.26 PHASIC LIQUID MASS FLOW AND LIQUID FRACTION DISTRIBUTION AT T=9.83 SECS FOR TEST S9 (15x8x2 GRID WITH AXIAL AND CIRCUMFERENTIAL BLOCKAGE)

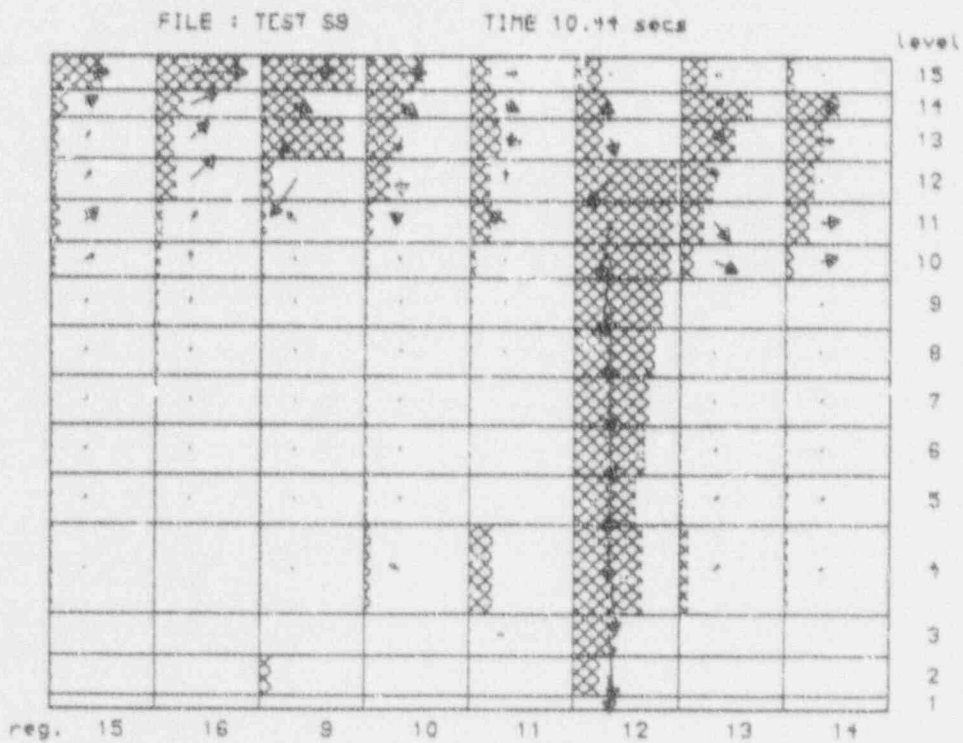


FIG. 4.27 PHASIC LIQUID MASS FLOW AND LIQUID FRACTION DISTRIBUTION AT T=10.44 SECS FOR TEST S9 (15x8x2 GRID WITH AXIAL AND CIRCUMFERENTIAL BLOCKAGE)

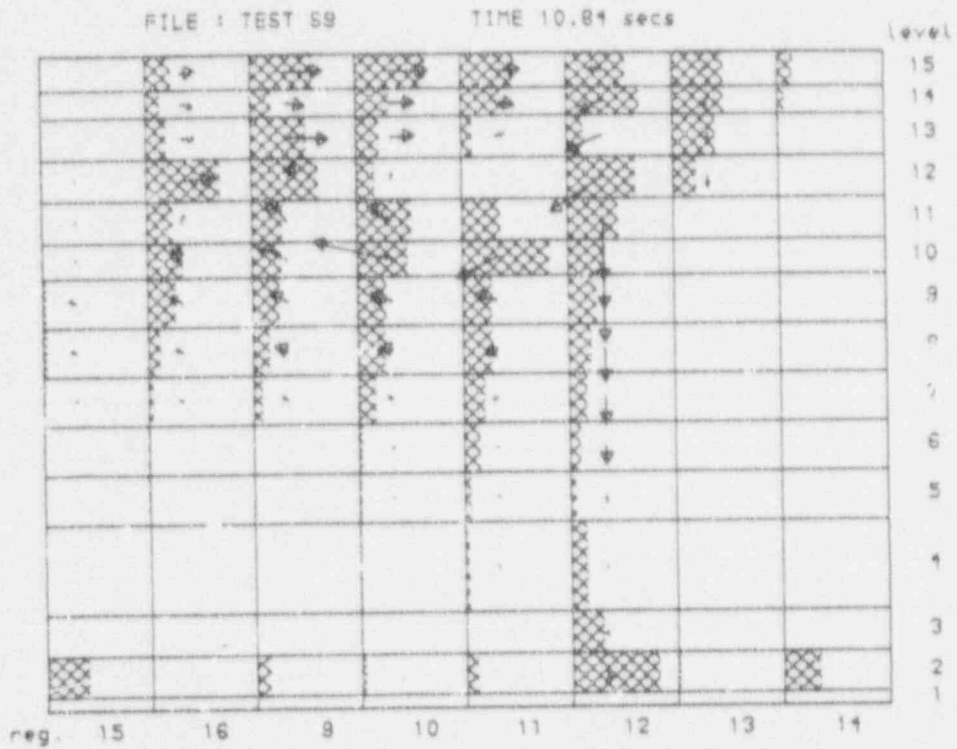


FIG. 4.28 PHASIC LIQUID MASS FLOW AND LIQUID FRACTION DISTRIBUTION AT T=10.84 SECS FOR TEST S9 (15x8x2 GRID WITH AXIAL AND CIRCUMFERENTIAL BLOCKAGE)

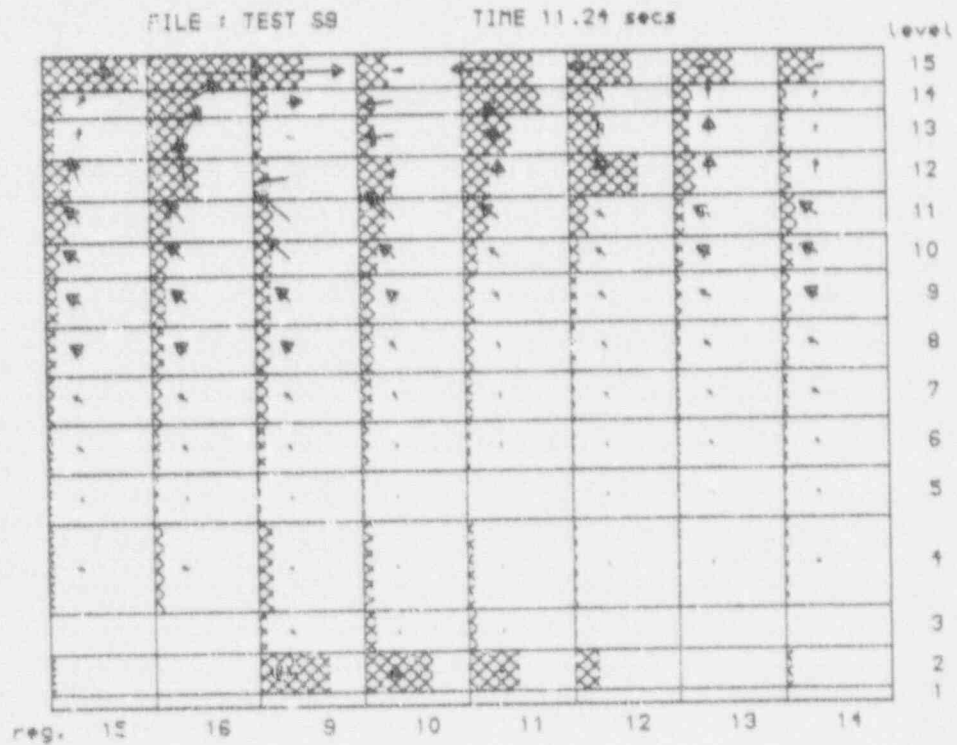


FIG. 4.29 PHASIC LIQUID MASS FLOW AND LIQUID FRACTION DISTRIBUTION AT T=11.24 SECS FOR TEST S9 (15x8x2 GRID WITH AXIAL AND CIRCUMFERENTIAL BLOCKAGE)

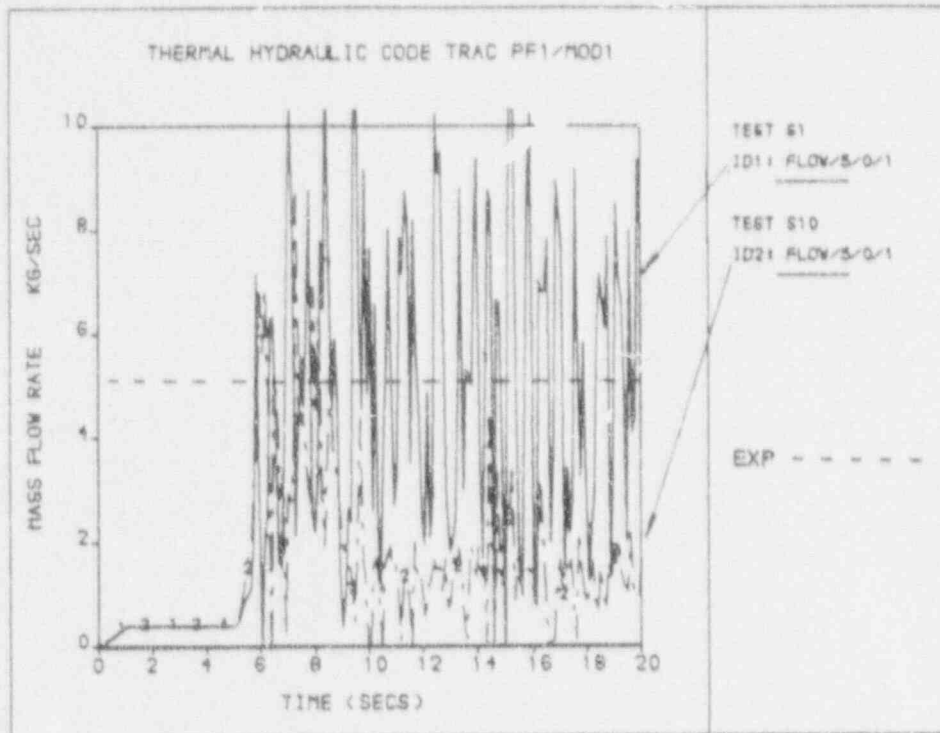


FIG. 4.30 BREAK MASS FLOWRATES FOR TEST S1 AND S10 (13.4:2 GRID)

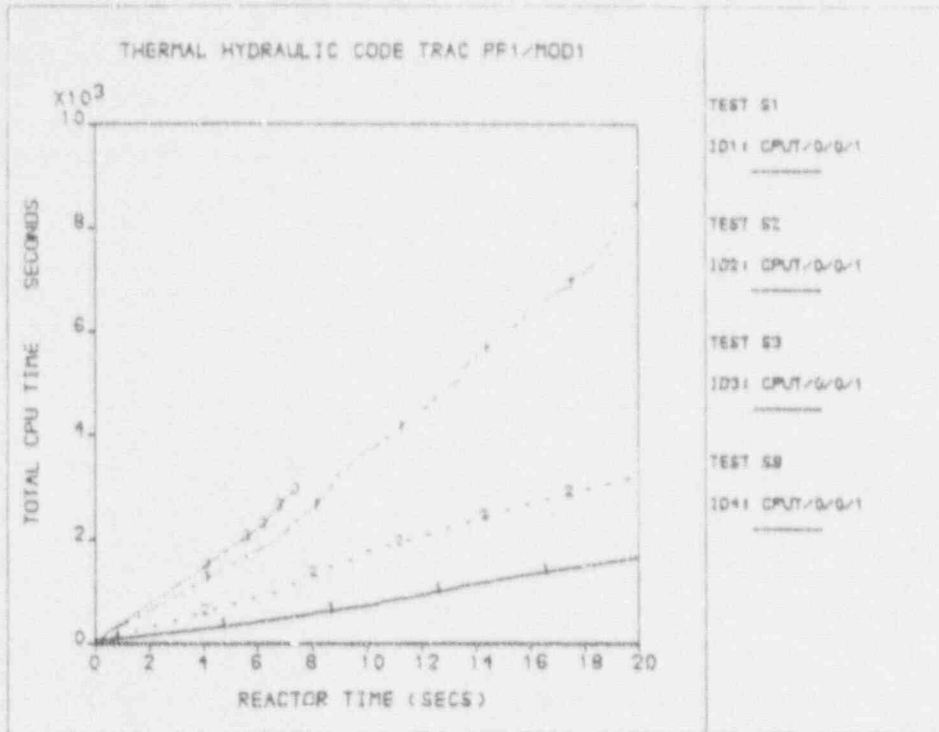


FIG. 4.31 COMPARISON OF TYPICAL CALCULATION CPU TIMES

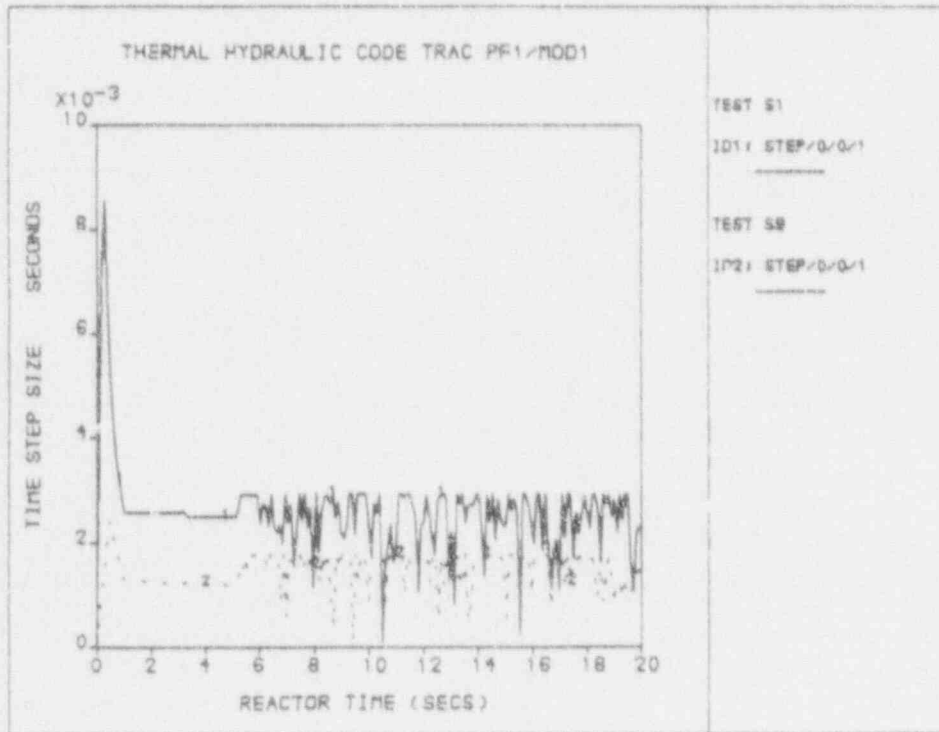


FIG. 4.32 TYPICAL CALCULATION TIME STEPS

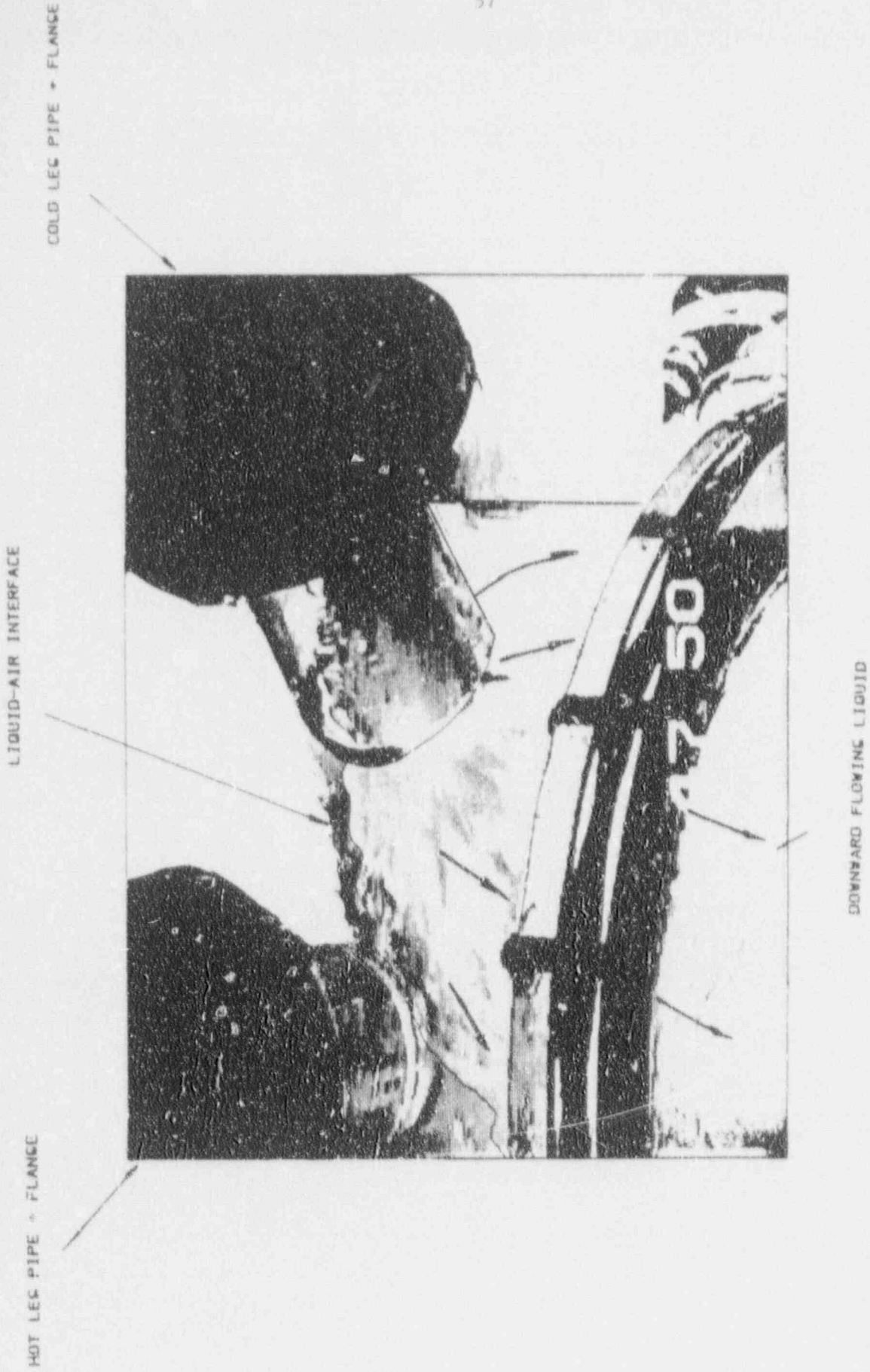


FIG. 4.33 LIQUID INJECTION IN 1/10 SCALE MODEL

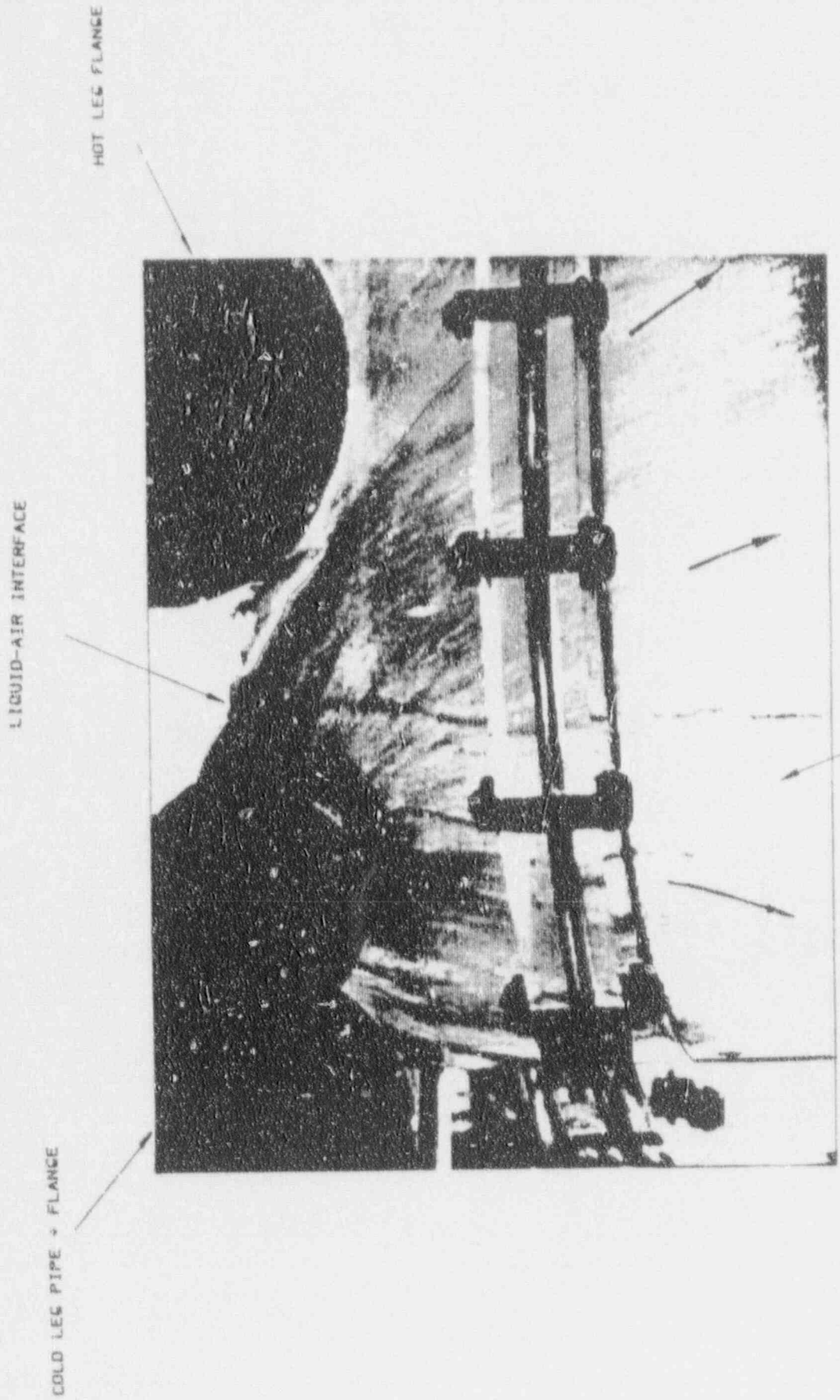


FIG. 4.34 LIQUID INJECTION IN 1/10 SCALE MODEL

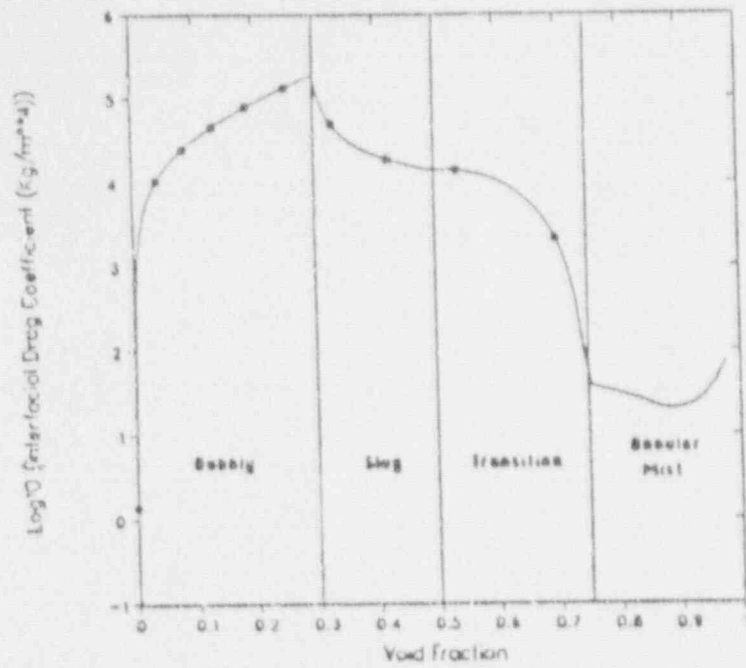


FIG. 4.35 TRAC INTERFACIAL DRAG CHARACTERISTICS OVER FLOW REGIME RANGE

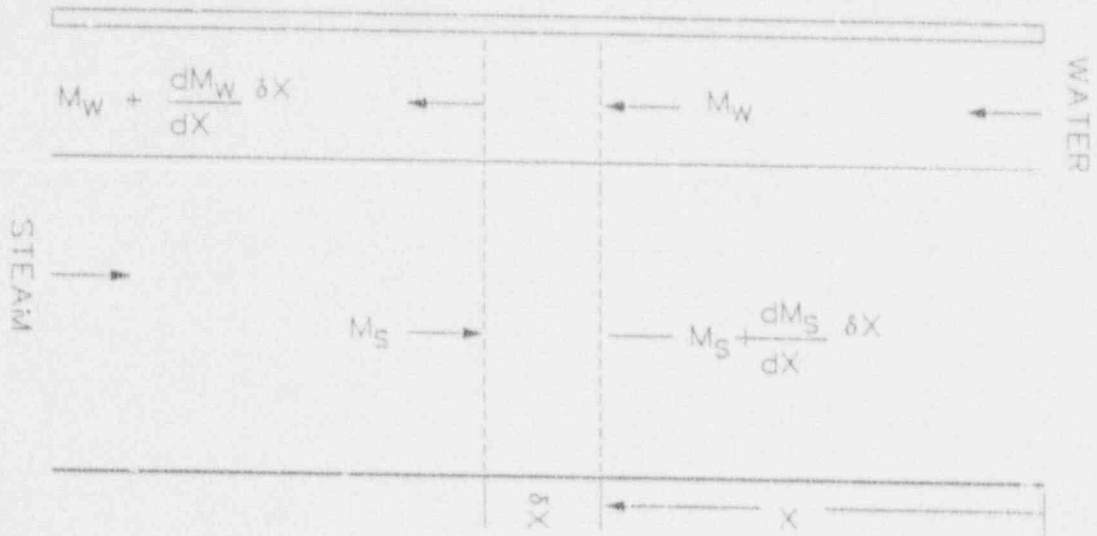


FIG. A.1 SCHEMATIC OF CONDENSATION MODEL

BIBLIOGRAPHIC DATA SHEET

(See instructions on the reverse)

REPORT NUMBER
(Assigned by NRC. Add Vol., Supp., Rev.,
and Addendum Numbers, if any.)

NUREG/IA-0053

1. TITLE AND SUBTITLE

An Assessment of TRAC-PF1/MOD1 Using Strathclyde 1/10 Scale
Model Refill Tests
2nd Report

3. DATE REPORT PUBLISHED

MONTH YEAR
March 1992

4. FINCH GRANT NUMBER

A4682

5. AUTHOR(S)

W. M. Dempster, A. M. Bradford, T.M.S. Callander, H.C. Simpson

6. TYPE OF REPORT

Technical

7. PERIOD COVERED (Include Dates)

8. PERFORMING ORGANIZATION - NAME AND ADDRESS (If NRC, provide Division, Office or Region, U.S. Nuclear Regulatory Commission, and mailing address. If contractor, provide name and mailing address.)

University of Strathclyde/Central Electricity Research Laboratories
Kelvin Avenue
Leatherhead, Surrey
United Kingdom

9. SPONSORING ORGANIZATION - NAME AND ADDRESS (If NRC, type "Same as above." If contractor, provide NRC Division, Office or Region, U.S. Nuclear Regulatory Commission, and mailing address.)

Office of Nuclear Regulatory Research
U.S. Nuclear Regulatory Commission
Washington, DC 20555

10. SUPPLEMENTARY NOTES

11. ABSTRACT (200 words or less)

TRAC-PF1/MOD1 predictions of LOCA Refill Experiments carried out on a 1/10 scale model are compared against experimental measurements and video observations. Sensitivity studies have been carried out to determine the effect of Hydraulic Diameter and nodalisation.

A simplified analysis of total penetration conditions reveals that the liquid head transfer coefficient during condensation is substantially greater than suggested by the reduction of the experimental measurements.

12. KEY WORDS/DESCRIPTORS (List words or phrases that will assist researchers in locating the report.)

ICAP Program, TRAC-PF1/MOD1, LOCA Refill

13. AVAILABILITY STATEMENT

Unlimited

14. SECURITY CLASSIFICATION

(This Page)

Unclassified

(This Report)

Unclassified

15. NUMBER OF PAGES

16. PRICE

THIS DOCUMENT WAS PRINTED USING RECYCLED PAPER

UNITED STATES
NUCLEAR REGULATORY COMMISSION
WASHINGTON, D.C. 20555

OFFICIAL BUSINESS
PENALTY FOR PRIVATE USE, \$300

SPEL - L FOURTH CLASS RATE
POSTAGE & FEES PAID
USNRC
PERMIT No. G-67

120555139531 1 1AM1C1
US NRC-OADM
DIV FOIA & PUBLICATIONS SVCS
TPS-PDR-NURFS
P-223
WASHINGTON DC 20555

NUREG/IA-003

AN ASSESSMENT OF TRAC-PTI/MODI USING STRATHCLYDE I/10 SCALE MODEL REFILL TESTS
2ND REPORT

MARCH 1992